# UTILIZATION OF FIBER LOOP RING DOWN TECHNIQUE FOR SENSING APPLICATIONS

A THESIS SUBMITTED TO
THE GRADUATE SCHOOL OF NATURAL AND APPLIED SCIENCES
OF
MIDDLE EAST TECHNICAL UNIVERSITY

BY

ALİM YOLALMAZ

IN PARTIAL FULFILLMENT OF THE REQUIREMENTS
FOR
THE DEGREE OF MASTER OF SCIENCE
IN
MICRO AND NANOTECHNOLOGY

JULY 2017

Approval of the thesis:

**UTILIZATION OF FIBER LOOP RING DOWN TECHNIQUE FOR SENSING APPLICATIONS**

submitted by **ALİM YOLALMAZ** in partial fulfilment and the requirements for the degree of **Master of Science in Micro and Nanotechnology, Middle East Technical University** by,

Prof. Dr. Gülbin Dural Ünver
Dean, Graduate School of **Natural and Applied Sciences** _____

Assoc. Prof. Dr. Burcu Akata Kurç
Head of Department, **Micro and Nanotechnology** _____

Assoc. Prof. Dr. Mehmet Fatih Danışman
Supervisor, **Micro and Nanotechnology, METU** _____

Assoc. Prof. Dr. Alpan Bek
Co-Supervisor, **Micro and Nanotechnology, METU** _____

**Examining Committee Members;**

Assist. Prof. Dr. Bülend Ortaç
UNAM, Bilkent University _____

Assoc. Prof. Dr. Mehmet Fatih Danışman
Micro and Nanotechnology, Chemistry Dept., METU _____

Assoc. Prof. Dr. Okan Esentürk
Chemistry Dept., METU _____

Assoc. Prof. Dr. İrem Erel Göktepe
Micro and Nanotechnology, Chemistry Dept., METU _____

Assoc. Prof. Dr. Alpan Bek
Micro and Nanotechnology, Physics Dept., METU _____

Date: 06/07/2017

**I hereby declare that all information in this document has been obtained and presented in accordance with academic rules and ethical conduct. I also declare that, as required by these rules and conduct, I have fully cited and referenced all material and results that are not original to this work.**

Name, Last name: **ALİM YOLALMAZ**

Signature : _____

## ABSTRACT

### UTILIZATION OF FIBER LOOP RING DOWN TECHNIQUE FOR SENSING APPLICATIONS

Yolalmaz, Alim

M.Sc.: Micro and Nanotechnology

Supervisor: Assoc. Prof. Dr. Mehmet Fatih Danışman,

Co-supervisor: Assoc. Prof. Dr. Alpan Bek

July 2017, 81 pages

Fiber loop ring down (FLRD) spectroscopy is based on multiple interaction of laser light with sample/analyte. It is evolved from cavity ring down spectrometer with addition of optical fiber. Measurement accuracy rises with multiple interactions and this enhances the minimum detection limit compared to other spectrometers using single pass interaction such as FTIR, UV-VIS spectrometer. The other advantages of this technique are its insensitivity to laser fluctuation and detector performance.

In this study, three FLRD set-ups were constructed with two laser sources at 800 and 1534 nm. Sensor regions were designed with two interaction methods as transmission and scattering and optimization for measurement parameters and probe structure were performed. The spectrometers' parameters were examined with chemicals such as ethanol, acetone, toluene, acetylene gas, nitrogen gas. The response of the spectrometers to sample/analyte were investigated and limitations were discussed. Finally, the performance of the spectrometers was compared with the literature.



Keywords: Fiber loop ring down spectroscopy, laser spectroscopy, evanescent field, microstructured fiber

# ÖZ

## FİBER HALKA DÖNGÜ SÖNÜMLEME TEKNİĞİNİN SENSÖR UYGULAMALARI İÇİN KULLANILMASI

Yolalmaz, Alim

M.Sc.: Mikro ve Nanoteknoloji

Danışman: Assoc. Prof. Dr. Mehmet Fatih Danışman

Ortak danışman: Assoc. Prof. Dr. Alpan Bek

Temmuz 2017, 81 sayfa

Fiber halka döngü sönümleme spektrometresi örnekle lazer ışığının çoklu etkileşmesine bağlıdır. Optik fiberin kavite halka sönümleme spektrometresine entegresiyle gelişmiştir. Ölçümün doğruluğu, örnekle lazerin çoklu etkileşmesiyle artar ve bu sayede, FTIR ve UV-VIS spektrometreleri gibi tek geçişli örnek etkileşmesine dayalı tekniklere kıyasla tespit limiti iyileştirilir. Lazerin şiddetindeki dalgalanma ve detektörün performansından bağımsız olması, bu tekniğin diğer avantajlarındandır.

Bu çalışmada, 800 ve 1534 nm dalga boylu iki lazer ile üç farklı fiber halka döngü sönümleme düzeneği oluşturuldu. Işığın iletimine ve saçılmasına bağlı olan iki etkileşme şekli ile sensor bölgesi tasarlandı ve ölçüm parametreleri ve sensor bölgesinin yapısın için iyileştirmeler yapıldı. Etanol, aseton, tolüen, asetilen ve nitrojen gazları gibi kimyasallarla spektrometre parametreleri incelendi. Spektrometrenin örneğe karşı tepkisi incelendi ve kısıtlamaları tartışıldı. Son olarak, spektrometrelerin performansı literatürle kıyaslandı.

Anahtar kelimeler: fiber halka döngü sönümleme, lazer spektroskopisi, süregelen dalga, mikro yapılı fiber

To my family and my little niece

## ACKNOWLEDGEMENTS

I believe that a M.Sc. candidate needs an understanding parent, perfect friends and an excellent supervisor, being a friend, a teacher and a family member. I am lucky because I have all three of them.

At the beginning, I would like to mention that I am so lucky because I have a family always supporting me even if my decision is bad. Thus, I myself learn how to decide and stand on my foot.

Then, I would like to mention I am very grateful to Assoc. Prof. Dr. Okan Esentürk. I am so happy to know him. Though he could not be my official supervisor due to bureaucratic reasons he guided me and shared his experience as if he was. He is the best model for everybody as not only a supervisor, but also a human being. He is so polite, helpful and thoughtful.

It was a pleasure to work with Assoc. Prof. Dr. Mehmet Fatih Danışman. He is kind, helpful and the most understanding person I know.

I thank to Farhad Hanifehpour Sadroud, Abu Sayed and Eser Torun for their contribution to my study.

I am so pleased to know my dear friends Mustafa Yaşa, Nurzhan Beksultanova, Adem Yavuz, Serkan Karadağ, Zühra Çınar, Yusuf Samet Aytekin, Nima Sohrabnia, Emine Kaya, Tuba Avcı, Duygu Tan, Tuğba Kapucu, Sinem Ulusan, Tolga Yaman, Özge İbiş.

This study was financially supported by TUBITAK grant no 212T079 and in part by METU BAP.

## TABLE OF CONTENTS

## LIST OF TABLES

TABLES

## LIST OF FIGURES

FIGURES

# CHAPTER 1

# INTRODUCTION

## 1.1. Brief description of FLRD technique

Optical fiber based sensors attract great interest due to their desirable features such as being fast, compact, sensitive and reliable in addition to having high resolution and low detection limit. Such an interest fuels development of highly anticipated, multi-functional optical fiber based measurement technique called fiber loop ring-down (FLRD) spectroscopy for uses in diverse application areas [1,2]. FLRD is a derivative of cavity ring-down technique and is using an optical fiber as a waveguide. It is a time domain spectroscopy technique in which a laser pulse is trapped in a fiber cavity with low losses enabling multiple interaction with the sample. FLRD technique finds applications in sensing of strain[3], refractive index[4], temperature[5], pressure[6], and most importantly in sensing of chemical[7] and biological species[8,9,10].

FLRD technique monitors decay of a laser pulse in the cavity due to inherent system component losses and absorption/scattering of the laser in sensor region as trapped laser pulse makes multiple rounds in the loop. This decay in general is monitored by ring down time (RDT) which is a specific duration corresponding to the time that passes for the incident laser pulse power to decrease to 1/e of its initial level. RDT depends on intrinsic fiber loss, coupler losses, splice losses, and characteristics of sensor region. One of the best advantages of FLRD technique is its insensitivity to laser power fluctuations and detector response[8]. Multiple passes of a pulse that is trapped in the cavity in an FLRD system increases interaction path length and secures stability of measurement result. Signals that are measured by a photodetector at each round carry the same information about sensor region thus FLRD promises a high sensitivity.

## 1.2. The set-up and equations

A typical fiber loop ring down setup consists of fiber optic cable, coupler, photodetector, isolator and sensor compartment as seen in Figure 1. With help of couplers, it traps laser light into a fiber loop, and the loop enables multiple interaction of laser light with sample in the sample compartment. Trapped light decays exponentially and carries information about intrinsic loss of the fiber loop such as couplers, splices, collimators, intrinsic fiber loss, and extrinsic loss of fiber loop such as sample absorption and scattering (an example of trapped light decay is seen in Figure 2).

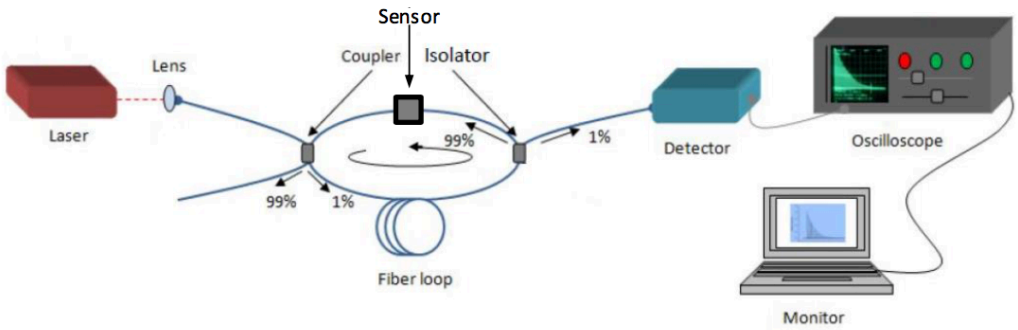


Figure 1. Conventional fiber loop ring down set-up

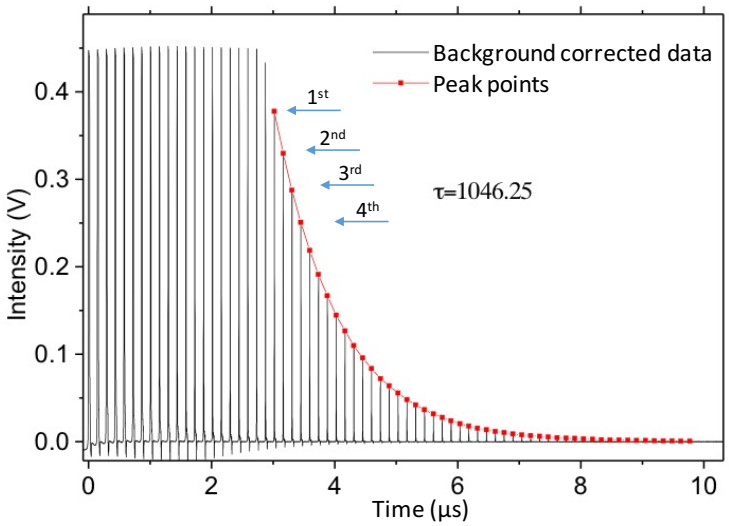


Figure 2. An illustration of decay of a trapped light in fiber loop

Intensity of a laser pulse (I) in the FLRD fiber loop is a function of time and depends on initial intensity ($I_0$), round trip time of the pulse ($t_{RT}$) and negative of the natural logarithm of total transmission through the fiber loop [-ln($T_{rt}$)]. Thus, the change of the laser pulse intensity in time is described as in Equation 1. After taking the integral of Equation 1 with respect to time, intensity of the laser pulse in terms of time is obtained as in Equation 2. (τ) in Equation 2 stands for the photon lifetime or ring-down time (RDT) and is the characteristic parameter of this technique.

$$\frac{dI}{dt} = -\frac{I*[-\ln(T_{rt})]*c_0}{n*L} \qquad \text{Equation 1}$$

$$I = I_0*e^{-t/\tau} \qquad \text{Equation 2}$$

RDT depends on round trip time and total transmission per round trip through fiber loop as seen in Equation 3. Moreover, it is insensitive to initial intensity. Round trip time is a function of effective refractive index of the fiber (n), length of fiber (L) and speed of light in vacuum ($c_0$), so it is given as in Equation 4.

$$\tau = \frac{t_{RT}}{-ln\,(T_{rt})} \qquad \text{Equation 3}$$

$$t_{\mathrm{RT}} = n*L/c_0 \qquad \text{Equation 4}$$

Total transmission loss –ln($T_{rt}$) in Equation 3 consists of information about sensor region, optical fiber and other loss sources. With detailed inspection of equation 3, others parameters can be specified as in Equation 5&6. They stand for intrinsic loss of optical fiber ($\alpha_f$), other losses due to splicings, couplers, etc. (B), and total loss in the sample compartment [-ln($T_{sensor}$)]. In direct interaction mechanism, as seen in Figure 3.a, gap for sensor region results in loss (referred to as [-ln($T_{gap}$)] in Equation 7) due to transmission of light through it even without sample/analyte. Absorption or scattering by sample/analyte contributes to total

sensor loss (given in Equation 7) and parameters related with them are extinction coefficient of analyte (ε), concentration of analyte (C) and interaction length through the sample cell (d). [2,1]

$$\tau = \frac{n*L}{c_0*[-\ln(T_{sensor})+\alpha_f*L+B]} \qquad \text{Equation 5}$$

$$-\ln(T_{rt}) = -\ln(T_{sensor}) + \alpha_f*L + B \qquad \text{Equation 6}$$

$$-ln(\mathrm{T_{sensor}}) = -ln\,(\mathrm{T_{gap}}) + \varepsilon*\mathrm{C}*\mathrm{d} \qquad \text{Equation 7}$$

1.3. Interaction mechanisms between laser and sample

There are two mechanisms for interaction of light with sample. One of them is that light meets sample in direction of propagation as seen in Figure 3.a&f. Other interaction mechanism is by means of evanescent field. This kind of interaction takes place after modification of optical fiber (Figure 3.b-e). Both of these mechanisms have different sensitivity and detection limit that depend on geometrical parameters and specifications of optical fiber. In direct interaction mechanism, intensity of light decreases either due to absorption or scattering of light by sample/analyte. Therefore, overall information about absorption and refractive index of sample/analyte are obtained when this configuration is used in FLRD set-up.

In addition to direct interaction of laser with sample in FLRD set-up, evanescent wave may be used to sense, detect and characterize chemical species. Evanescent wave is a phenomenon takes place at the boundary where total internal reflection of a ray occurs. The evanescent field penetrates through low refractive index medium from high refractive index medium. Field's intensity decays exponentially with distance from the interface where the field emerges (Equation 8). Thus, it can be used to investigate optical properties of medium such as refractive index and absorptivity at the surface of medium. Sensing, detection or characterization of sample/analyte at the interface happens with either cavity ring down or fiber loop ring down technique.[11,12] Evanescent field of the core mode

occupies the cladding region of fiber; therefore, field needs to be extended outside of the cladding region. This can be achieved by side-polishing, tapering or etching the optical fiber as shown in Figure 3.b-d.[1] Evanescent wave leaks to low refractive index medium when it propagates through a section of optical fiber. It interacts with the surrounding medium in case it has penetration depth ($d_P$) longer than cladding thickness of fiber. Strength of field is a function of refractive index of cladding and surrounding medium, the angle which ray reflects at the interface of cladding and surrounding medium and wavelength of laser as seen in Equation 9.[11]

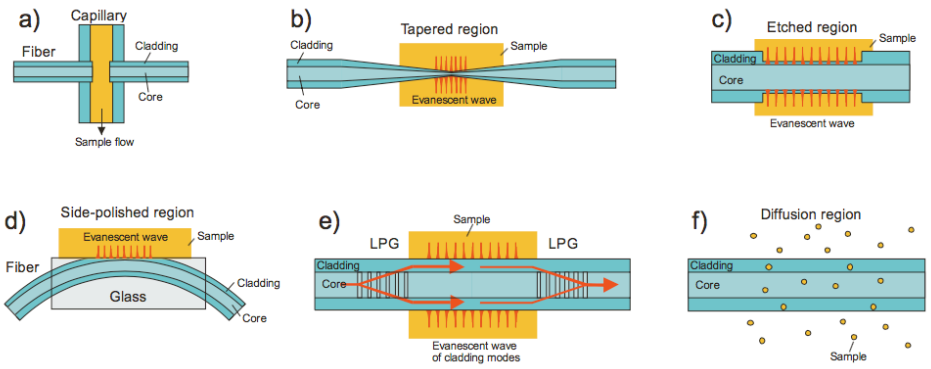


Figure 3. Various form of probes used in fiber loop ring down spectroscopy. (a) A gap in the fiber for direct interaction of light with sample. (b) In a tapered fiber, mode in the core transfers to mode in the cladding, so the evanescent field extends outside the fiber. (c) By etching the cladding of optical fiber, the evanescent field penetrates into sample/analyte. (d) With side polished fiber, the evanescent field interacts with surrounding material (e) Using long-period gratings (LPGs), pulse can be directed to the cladding region and the evanescent field interacts strongly with sample. (f) Small gas molecules such as $H_2$ can diffuse into the fiber and intensity of light changes. [1]

$$d_p = \frac{\lambda}{2\pi\sqrt{{n_1}^2 sin\theta\text{-}{n_2}^2}} \qquad \text{Equation 8}$$

Intensity of detected signal at FLRD set-up changes with intensity of evanescent field. Intensity of evanescent field shows difference either due to morphology where field interacts with surrounding medium or optical properties of surrounding medium around optical fiber, that is, optical properties of sample. The surface roughness causes scattering of evanescent field, so detected signal decreases.[13] However, with the same probe surface, optical properties of different samples may be compared. Secondly, optical properties of sample tunes amplitude of evanescent field because, the sample causes scattering of evanescent field due to sample having different optical characteristic such as plasmon frequency, extinction coefficient, refractive index. In addition to that, detected signal does not show linear behavior with refractive index of sample, so is sensitivity of the FLRD technique.[4]

## 1.4. Optical fibers

Optical fiber is made up of silica glass and it has core and cladding regions. Light undergoes total internal reflection in case refractive index of core is greater than refractive index of cladding. Light propagates in the form of modes through fiber. A single mode is permitted in case the core diameter is small. Fibers with large core diameter are called as multimode fibers. In both single mode and multimode fiber, refractive indices in core and cladding do not change across the cross section. In graded-index fiber, refractive index of the core changes across the cross section (Figure 4).[14] These kind of fibers are used in FLRD technique.

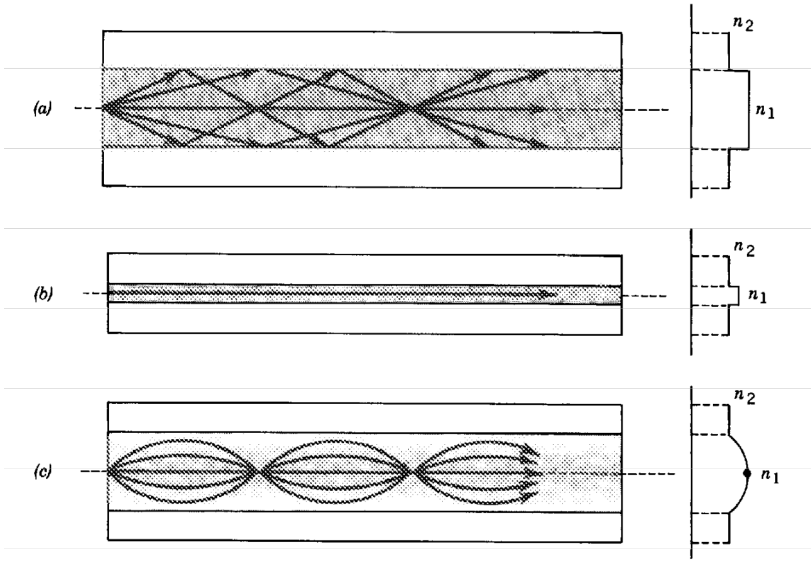


Figure 4. Geometry, refractive index profile, and typical rays in: (a) a multimode step index fiber, (b) a single mode step-index fiber, and (c) a multimode graded-index fiber[14]

In addition to these fibres, there are many kinds of fibres which may be used in FLRD technique and photonic crystal fiber (PCF) is one of them. Photonic crystal fiber has remarkable properties due to the fiber structure with lattice of air holes running along its length. Index-guiding PCF and photonic bandgap PCF are kinds of PCF. Index-guiding PCF has a solid core and light guiding is based on total internal reflection due to the fact that effective refractive index of cladding region is lower than that of core region. The second kind of PCF has a hollow core and the presence of photonic bandgap at a specific range of wavelength in the cladding region helps to guide light. Light reflects from each layer in the PCF and this structure keeps light confined in the lower index core. This structure is formed by a periodic wavelength-scale lattice of microscopic holes in the cladding region (Figure 5).[15] However, integration of these fibers in FLRD setups is not as simple as single mode step index fibers.

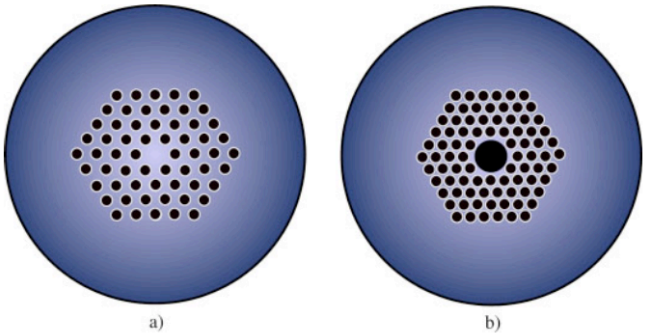


Figure 5. Structure of photonic crystal fiber: a) index-guiding PCF; b) photonic bandgap PCF.[15]

The difficulty of fusion splicing PCF to conventional step index single mode fiber arises due to structure of these fibers and mode field mismatch. The geometry of PCF is very sensitive to deformation under a low thermal energy.[16] Filament based fusion splicers may be used to join these type fibers, but they are expensive.[17] A simple recipe for splicing PCF to step-index SM fiber using a conventional arc fusion splicer exists in the literature, but this recipe is optimized for a specific arc-fusion splicer (Ericsson FSU-995) and should be modified/optimized if a different splicer (like the Fujikura FSM-60S in our laboratory) is used.[16] Thus, finding splicer parameters giving low loss and performing splicing without collapsing the structure of PCF is necessary for a good permanent joint. Furthermore, it enables to create a few millimeter-long sensor region for in-situ applications.

## 1.5. Application examples

With its great potential FLRD has already found applications in numerous areas with its aforementioned unique properties. One of the first applications of FLRD was in telecommunication, where optical loss is a very important issue and must be low for long distance information transmission. Here, loss measurement less than 0.1% is quite difficult with usual techniques and with its multi-pass nature FLRD was used to measure optical loss due to coupler, optical fiber, and

fiber splice with great accuracy[18]. Another area where FLRD finds application is in monitoring of global warming gases. Global warming gases such as $CO_2$, $CH_4$ and CO are detectable with gas chromatography but remote detection is not yet possible, thus, FLRD spectrometer has potential to sense global warming gases remotely[19]. FLRD recently finds application in detection of chemicals and their concentrations as lasers become available in different colors suitable for the chemical identification. A commonly used chemical during instrument development is acetylene for testing spectrometer's stability and sensitivity at around 1534 nm. Zhang et al. used erbium doped fiber amplifier (EDFA) and fiber Bragg grating (FBG) in their FLRD spectrometer set-up to increase the sensitivity and were able to detect 1% acetylene with a 1 cm long sampling cell[20]. With a 3 km optical fiber and 25 cm gas cell FLRD setup, Zhao et al. were able detect 0.1% acetylene with 1.02% stability and 0.18% single point reproduciblity[21]. Andrews et al. also used EDFA in addition to band pass filter on a nested loop in their FLRD setup for detection of acetylene in helium at 1532 nm using phase shift method and could quantify 50 ppm acetylene in helium[22]. Similarly, with an introduction of EDFA and FBG to their setup with a 65 mm long gas cell Zhao et al. were able to detect 0.1% acetylene in $N_2$ with a deviation of less than 0.4%[23]. Moreover, using a 1.15 m photonic bandgap fiber (PBGF) as a gas cell, Brakel et al. created a compact sensor region for detection of 3% $C_2H_2$ in a nitrogen mixture. In this FLRD configuration, two EDFAs were used in addition to FLRD configuration.[24]

With evanescent field interaction, FLRD is used for similar purposes mentioned above. There are few studies related with FLRD using evanescent field (EF-FLRD) based interaction in literature. Kaya et al. studied sensing of water embedded in concrete using longer than 15 cm etched optical fiber after integration of fiber to FLRD spectrometer with 1515 nm wavelength laser.[25] Herath et al. reported sensing of DNA and bacteria using similar set-up configuration with 120 meter fiber loop for evanescent field interaction. Sensor unit is created by etching of 24 cm long section of fiber down to 10 μm using HF acid and fast response ( <1 second) to the change in the external media is achieved with 1515.15 nm

wavelength laser.[10] Alali et al. used EF-FLRD, consisting of similar sensor items to those used in this study, as relative humidity sensor in a dynamic range of 4% to100% at a constant temperature. The sensor head is formed by etching 12-20 cm optical fiber and relative humidity change due to refractive index change is monitored with 1515.25 nm laser with fast response (≈1 s). [26] Moreover, EF-FLRD sensor was designed as glucose sensor (glucose concentrations ranging from 0.1% to 1%) by using 1515.25 nm laser and etched optical fiber whose length varies from 10 to 22 cm. Wang et al. obtained 0.1 s response time for glucose solution and they were also able to discriminate signals for with and without DI water.[27] Wang et al. also designed an EF-FLRD sensor using 1515.25 nm wavelength laser and showed difference between RDTs of air and water with etched optical fiber of 1.5 cm long and 17.7 μm diameter.[12] Ittiarah et al. detected NaCl and glucose ($C_6H_{12}O_6$) solutions using EF-FLRD with 1550 ± 25 nm laser after side polishing of 12 mm optical fiber. Moreover, their sensor operates between 1.34 and 1.38 in terms of refractive index unit.[4] Using tapered fiber having 10 μm waist diameter and 28 cm length, Tarsa et al. were able to detect 1-octyne using FLRD with laser scanning from 1520 to 1550 nm.[28]

However, there is still much room for improvement both in sensitivity and in simplification of the FLRD set-ups toward development for commercial use of the instrument. For instance, the effect of sample gas pressure in the sensing region on the system sensitivity have not been studied before. This may have important implications for designing FLRD systems with pre- or on site-concentration capabilities. Moreover, either detection of absorbent or non-absorbent species in visible range of electromagnetic spectrum has not been studied.

In this study, firstly, a sensitive intracavity based FLRD spectrometer with 1534 nm laser is introduced. Then, its application on quantitative detection of acetylene with high reproducibility and low deviation in RDT is presented. The spectrometer has a simple configuration and is constructed from commercial low cost components. In addition, sensing region of the instrument was designed to allow high pressures, which makes it possible to increase the concentration of the

analyte by increasing the amount/pressure of the sample gas. The following sections describe FLRD spectrometer's sensor region, data collection procedure, data processing, and instrument stability along with its application on acetylene detection. In the second part of the thesis, the unique design of a FLRD spectrometer using 800 nm laser source is presented with electro-optic, optoelectronic, and optic items. Performance of this spectrometer was increased by preparation of etched optical fiber as sensing unit and detection of different liquid samples were studied. Finally, nanoscale thick films (made up of polymer and silane) were deposited on the surface of etched sensing region in order to detect their formation/thickness.

# CHAPTER 2

# EXPERIMENTAL

In this section, the construction of three different fiber loop ring down spectrometers with two different laser sources are discussed in detail. Firstly, data acquisition and processing procedures, which are common in both set-up is presented. Next, the FLRD set-up with laser at 1534 ± 6 nm wavelength is mentioned in details. Then the performance of the spectrometer is discussed. Afterward, application of etched optical fiber with evanescent field based interaction between laser and liquid sample such as ethanol, acetone, DMF, etc is presented. In the second part, the configuration of FLRD with laser at 800 nm wavelength is mentioned and optimized measurement parameters with/without sample are discussed. In addition, coating of etched fiber with either polymer or organic films to detect nanoscale films and to improve the performance of the spectrometer is discussed. Later, etching studies performed for evanescent field interaction is discussed and the etching studies are mentioned. Lastly, our work on splicing of photonic crystal and microstructured fibers to single mode fibers are mentioned with important splicing parameters and fiber specifications. All spectroscopic measurements with FLRD technique mentioned here are carried out at 19±2 °C and atmospheric pressure (Three spectrometers are located in Okan Esentürk's research laboratory, Chemistry department, B-48, Middle East Technical University, Ankara/Turkey). The whole study for etching optical fiber is done at room temperature in the hood in Fatih Danışman's research laboratory (Chemistry department, B-17, Middle East Technical University, Ankara/Turkey).

## 2.1. Data analysis

Here, the procedure of data analysis to obtain ring down time (RDT) is presented. Firstly, the photodetector transfers signal levels to the oscilloscope and data is recorded with help of a Matlab code. Each data set is collected with 512 averages at a 50 Ω terminated input in the oscilloscope. Voltage scale is determined by observation of the highest signal-to-noise (S/N) with lowest standard deviation while maintaining the largest dynamic range. 50 mV voltage division is used for FLRD with 1534 nm wavelength laser and 1 mV voltage division is used for FLRD with 800 nm wavelength laser.

Inset in Figure 6.a presents a representative data of the pulse intensity after each round, forming a pulse train. It is seen that the signal level of each pulse follows an exponential decay as expected due to the inherent losses of the instrument components at each round. Once the data is collected the background response of the detector is identified as in red trace which is due to the detectors inherent response. Even though the detector response did not have a significant contribution to the signal level recorded as seen in the actual data given in the inset, it is corrected as follows. The data corresponding to the detectors response is separated and fitted to an exponential (Figure 6.b). The experimental data (now on called data) is then corrected by subtracting the fit from the collected one (Figure 6.c). Next, the peak amplitude of each pulse in the data is determined. The first 9 peaks were discarded since they were out of scale in the 50 mV voltage scale of the oscilloscope. Finally, the peak points are fitted to equation 2 (discussed in the introduction) to extract the RDT (Figure 6.d).

The data presented in Figure 6 is for $N_2$ at 25 psia in the sensor region with a ring down time of 485.4 ± 0.6 ns or 1.3152 ± 0.0016 dB loss per round trip. The ring down time and corresponding loss of the closed loop, without a sensor region, are 1046.3 ± 0.8 ns and 0.5977 ± 0.0004 dB, respectively, (see Figure 2 for decay train of incident pulse through the closed loop).

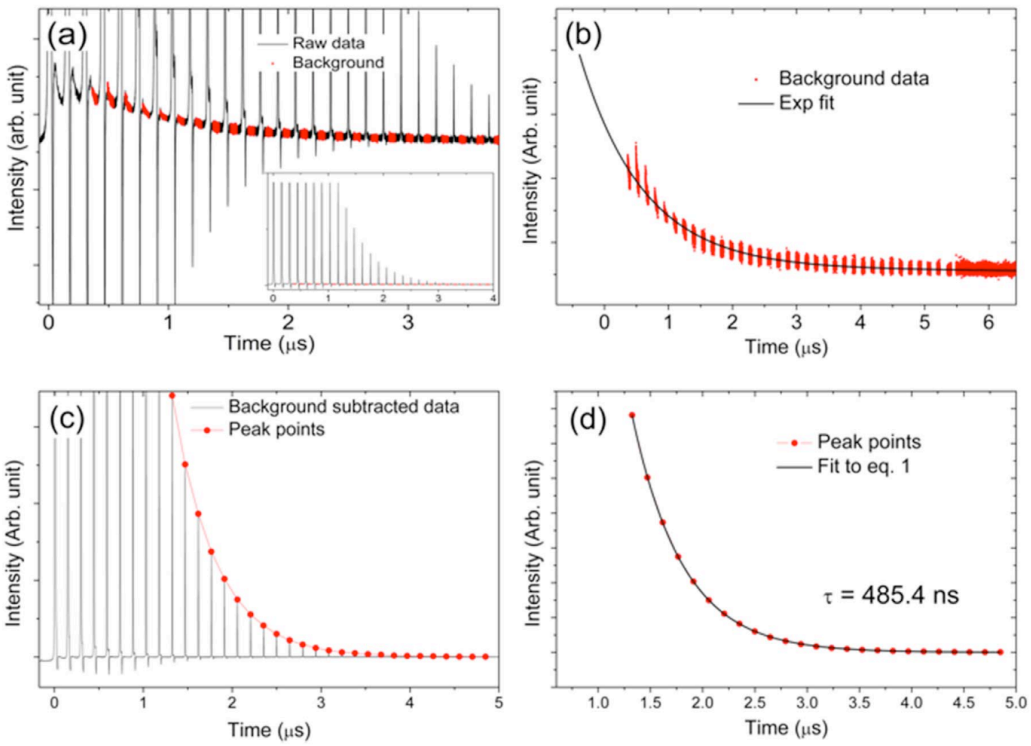


Figure 6. Data processing example with 25 psia pure $N_2$ in sampling compartment. (a) A zoom in on the background region of the experimental data (the full data is shown in the inset), (b) background data with the fit curve, (c) background corrected data with peak points, (d) peak points and their fit to an exponential function given in Equation 2

## 2.2. FLRD set-up with 1534 nm wavelength laser

In this section, construction of FLRD spectrometer with 1534 ± 6 nm wavelength laser is discussed. First, the construction of sample compartment is mentioned with parameters of sensor unit. Later, sensing of gas samples with the direct interaction of laser is performed. Furthermore, evanescent field based interaction with liquid samples are studied after preparation of etched optical fiber.

### 2.2.1. The set-up

The FLRD set-up is constructed with a 4 ns pulsed, 1534 nm (6 nm FWHM) laser (Cobolt Tango) operating at 3 kHz, a fiber coupled lens, 25 m single mode step-index fiber, 99:1 coupler, isolator, a sensor region (0.718 ± 0.002 dB calculated loss) created by two collimators (Thorlabs 50–1550 A), two photodiodes (EOT 3010, DET08CFC), and an oscilloscope (Tektronix MSO 4104).

The spectrometer configuration and the sensor region details are given in Figure 8. In the FLRD set-up, the laser pulse from free space is guided to fiber via fiber-coupled lens. One percent of the laser pulse is coupled to the cavity with a coupler and guided to the sensor region. The rest of incident laser power is directed to a photodiode and used as trigger for the oscilloscope. After the pulse passes through the sensor region, 1% of the light travelling in the cavity is directed to a second photodiode by an isolator for recording the signal level at each round trip. The rest is directed to the loop for multiple pass through the sample region until all the light in the loop decays. The secondary purpose of the isolator is to prevent the back reflection off of the collimator reaching to the photodiode. The detailed items list is given in the Table 1.

The fiber loop length should be decided by considering constrains such as laser repetition rate, pulse duration, and number of peak points, which is important to obtain low deviation in measurement parameter. The laser repetition rate limits the maximum length of fiber loop. The length should be chosen to prevent overlap of adjacent pulses. Secondly, pulse duration is used to determine the shortest fiber loop that can be used to construct FLRD set-up. The shortest fiber loop (L) is calculated by using Equation 9. The effective refractive index of fiber (n) and pulse duration ($\Delta t$) are the variables in this equation. Lastly, the number of peak points that results in the lowest deviation in RDT should be chosen. This parameter is influenced by the detector performance, average setting of the oscilloscope, fiber loop length and total loss seen in the FLRD set-up. Therefore, before construction of any spectrometer, total loss due to equipment should be determined to find

optimum fiber loop length. For this purpose, a fiber length range should be described by using number of available peak points. Using the effective refractive index of optical fiber (It is calculated by using measured fiber loop length and round trip time seen in the experiment for closed loop) and total loss due to items such as coupler, collimator, and intrinsic loss of optical fiber, a graphical demonstration was prepared to see the effect of fiber loop length on the ring down time and number of peak points. In Figure 7.A it can be seen that RDT increases with increasing fiber loop length. Relative standard deviation in RDT is related reciprocally with RDT, so, higher RDT gives lower deviation. However, number of peak points decreases with fiber loop length and number of peak points does have significant effect for calculation of RDT with high accuracy (Figure 7.B). In addition to that, number of peak points and fiber loop length are not able to be decided without preliminary experiments because contribution of known and unknown parameters on error in RDT calculation. Therefore, after calculations of relative standard deviation of RDT for different fiber loop lengths, suitable loop length is found.

$$L = \Delta t^{*} c/n \qquad \textit{Equation 1}$$

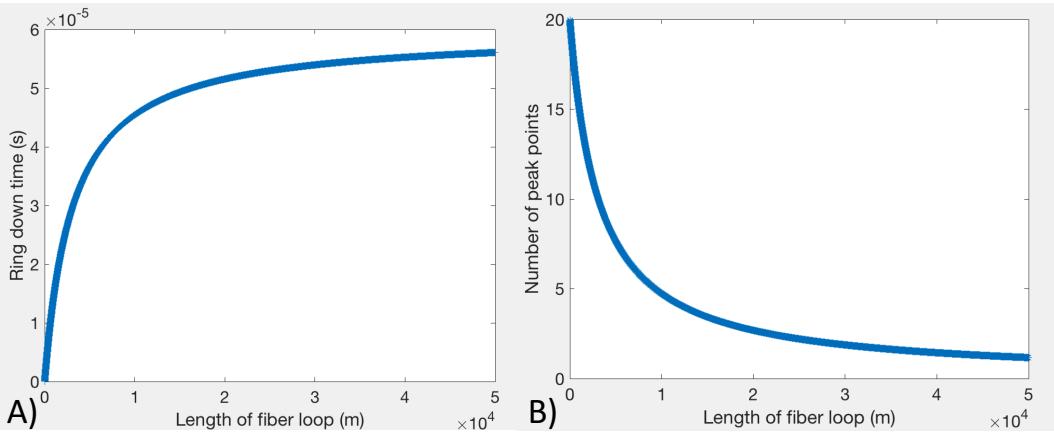


Figure 7. Graphical demonstration for deciding fiber loop length

One of the main factors determining the ring down time (and sensitivity in part) of the spectrometer is the path length of the sensor region. The loss increases significantly when the distance between the collimators is beyond a certain length due to diverging/ scattering light after the first one. Thus, the optimized distance is found to be 9 mm for the highest sensitivity while keeping the loss as low as possible and increasing interaction length of light with sample. Regardless, the two collimators add extra loss compare to the closed loop like pair insertion and insertion losses, which is less than 0.33 dB at 9 mm separation. The sensor region is sealed with a plexi-glass housing to which collimators are fixed by epoxy glue and gas inlet and outlet ports are fixed by high pressures fittings. The decay train is monitored and the collimators are constantly aligned during curing stage of the epoxy. Once dried, the sampling region is checked for gas leakage.

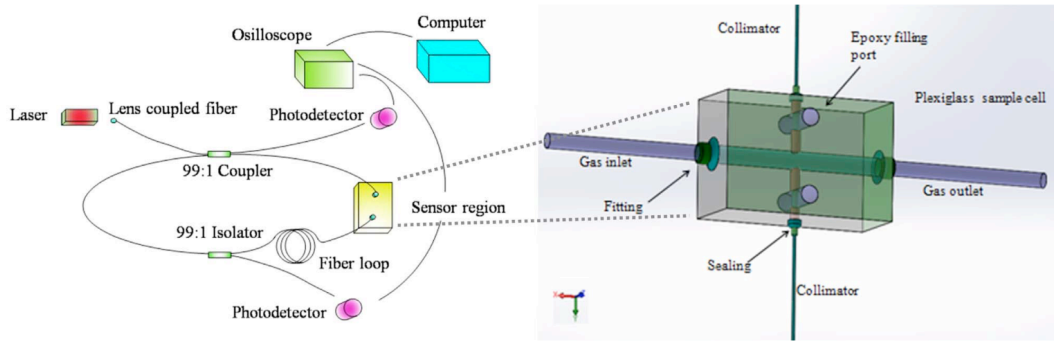


Figure 8. Schematic configuration of the intracavity FLRD spectrometer (left) and the sensor region (right).

Table 1. The equipment used for FLRD with 1534 nm laser

| **Item** | **Manufacturer** | **Specification** |
|---|---|---|
| Laser | Cobolt Tango | 1534 nm central wavelength, 6 nm FWHM, 4 ns pulse duration, 3 kHz rep. rate, 13.6 mW average power, 4.53 μJ pulse energy |
| Fiber optic cable | Oz Optic | 8.2 μm core diameter, 125 μm cladding diameter, 0.35 dB/km intrinsic loss @ 1550 nm |
| Isolator | Lightel | TIS-01-A-B-0, hybrid 1550 nm 1% tap coupler |
| Coupler | Lightel | SWC-22-P-9901-H-1-B-0 |
| Oscilloscope | Tektronix | MSO 4104 |
| Photodetector | Thorlabs | DET08CFC |
| Photodetector | Newport | EOT 3010 |
| Collimator | Thorlabs | 50–1550 A |

### 2.2.2. Gas samples and stability measurement

In this section, laser spectrum and the specification of gas samples are presented. Then, experimental procedure for measurement of RDT such as number of averaged RDT, RDT collection interval, operating pressure range is mentioned in detail.

Acetylene absorption spectrum and laser emission spectrum are presented in Figure 9. Nitrogen ($N_2$, 99.99%), acetylene ($C_2H_2$, 98%) and 0.1%, 1%, 5%, and 10% (v/v) $C_2H_2$ in $N_2$ gas mixtures were purchased from Linde Inc. and used as is without any further purification. The mixture gases have 2% tolerance in $C_2H_2$ amount.

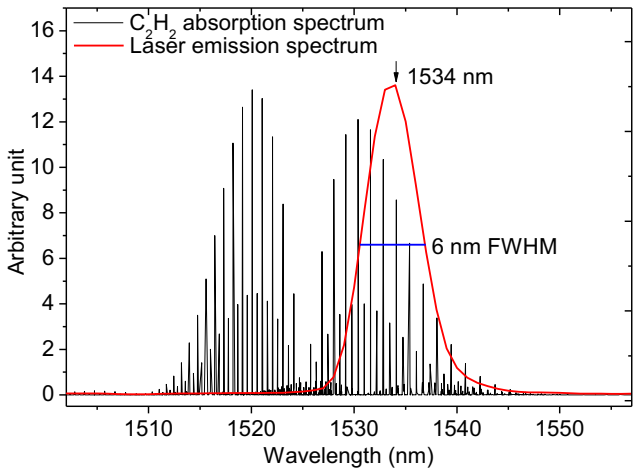


Figure 9. Laser emission spectrum and acetylene absorption lines

Each data is collected as follows: 5 pulse trains are collected with 5 s intervals each with 512 scans averaged by the scope, and an average RDT is calculated as average of these five pulse trains` RDTs. This procedure is applied for reference $N_2$, all mixtures, and pure acetylene at each pressure between 25 psia and 65 psia at 10 psia increments. The lowest pressure of 25 psia was chosen because of the lowest adjustable value on the pressure gauge and the highest pressure of 65 psia is the experimental limitation that can be attained with this setup before fracturing sample compartment and/or the collimators.

### 2.2.3. Liquid samples and sensor region

The sensor unit for FLRD spectrometer at 1534 nm in this section is formed with etching process (See Section 2.4 for details of etching procedure). After preparation of etched fiber, it is integrated to the spectrometer for sample measurement. The schematic configuration of the spectrometer is depicted in Figure 10. The spectrometer is tested for its accuracy, stability, repeatability with ethanol, acetone, DI water, DMF, DMSO, etc. Before measurement of each sample's RDT, rinsing of the probe with the same sample which is in different beaker is done. The high fluctuation in the RDT values observed in initial

measurements (discussed later in detail in section 3.2, Figure 37) were thought to be caused by the slight motion of the etched fiber while the probe is being lowered in the fixed sample beaker (configuration 1). Therefore, to eliminate this problem, following experiments (discussed later in detail in section 3.2, Figure 38 & Figure 39) were performed by keeping the probe fixed and moving the sample (beaker) toward the probe (configuration 2).

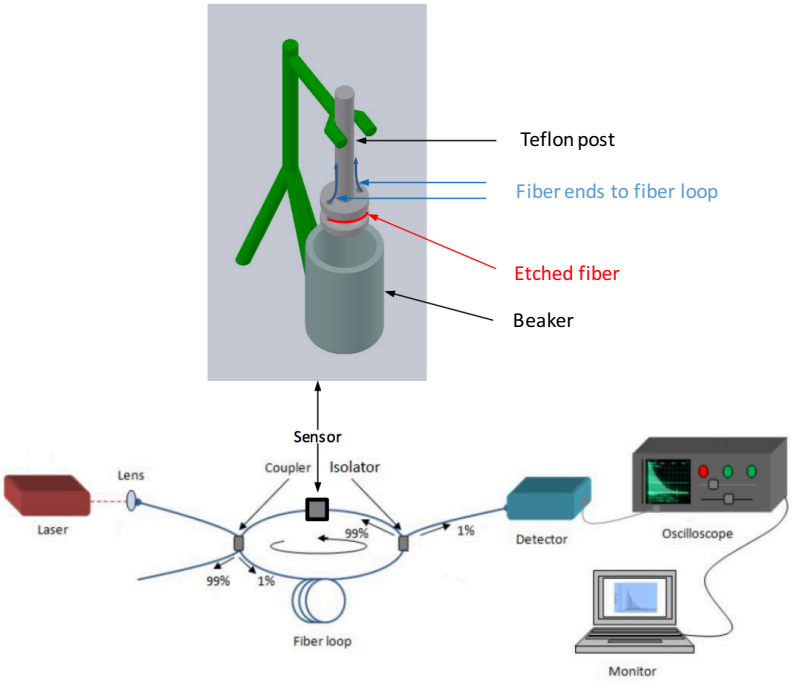


Figure 10. FLRD spectrometer at 1534 nm with the etched optical fiber

## 2.3. FLRD set-up with 800 nm wavelength laser

In this section, details of the spectrometer at 800 nm wavelength is discussed first. The equipment used to form the set-up is listed in Table 2 and laser emission spectrum is presented in Figure 11. Next, the measurement parameters are reported with/without sample for the best S/N ratio and reproducible measurements. Then, the procedures for liquid sample measurements and organic film coating are discussed after integration of etched optical fiber (Length range is 4-9.8 cm, diameter range is 8.5-47 μm) to the FLRD set-up at 800 nm.

Table 2. Equipment for FLRD set-up at 800 nm

| **Item** | **Manufacturer** | **Model** | **Detail** |
|---|---|---|---|
| Ti:Sapphire Laser | Coherent | Mantis-5 | 80 MHz repetition rate, 100 fs pulse duration, broadband emission |
| Fiber coupler | Lightel | SWC-22-P-9901-H-1-B-0 | @ 808 nm, 2x2 ports, 98:2 splitting ratio |
| Optical fiber | Nufern | 780HP | Intrinsic attenuation ≤ 4 dB/km @ 780 nm |
| Detector | NKT | 818-BB-45F | GaAs, Wavelength 400-900 nm, Fall time < 30ns, Bandwidth(- 3 dB) 12.5 GHz |
| Oscilloscope | Tektronix | MSO4104 | 5 GHz repetition rate |
| Power meter | Thorlabs | PM100D | Wavelength range: 185 nm - 25 μm, Power range: 100 pW to 200 W |
| Power sensor | Thorlabs | S310C | Wavelength range: 0.19 - 25 μm, 10 W |

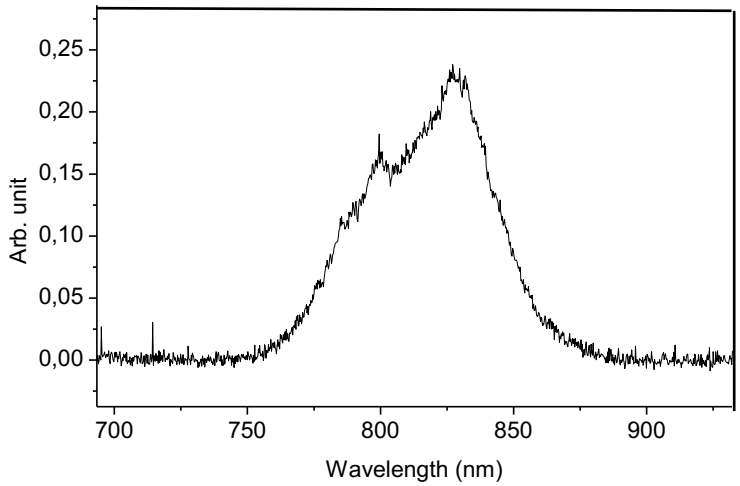


Figure 11. The spectrum of mode-locked laser used at the FLRD at 800 nm

2.3.1. The set-up and optimization of spectrometer's performance

The 800 nm laser source in the laboratory has 80 MHz repetition rate and this means a pulse enters into the fiber loop at each 12.5 ns. This low period of the laser is not suitable to observe the decay train of a pulse because, following pulses overlap in the fiber loop. Thus, the repetition rate of the laser was decreased to a lower value by using a Pockels cell (Figure 12). The laser pulse has s-polarization and it is not suitable for operation of the Pockels cell. Therefore, p-polarization of pulse is obtained by rotating the polarization with a half wave retarder. Then, Glan-Thompson prism is used to filter leaking s-polarized pulse. Next, pulse enters the crystal of the Pockels cell and is rotated to s-polarization at a specified rate (This value is easily controlled with the knob of the driver). After the repetition rate is set, fiber loop ring down spectrometer is ready to monitor decay train.

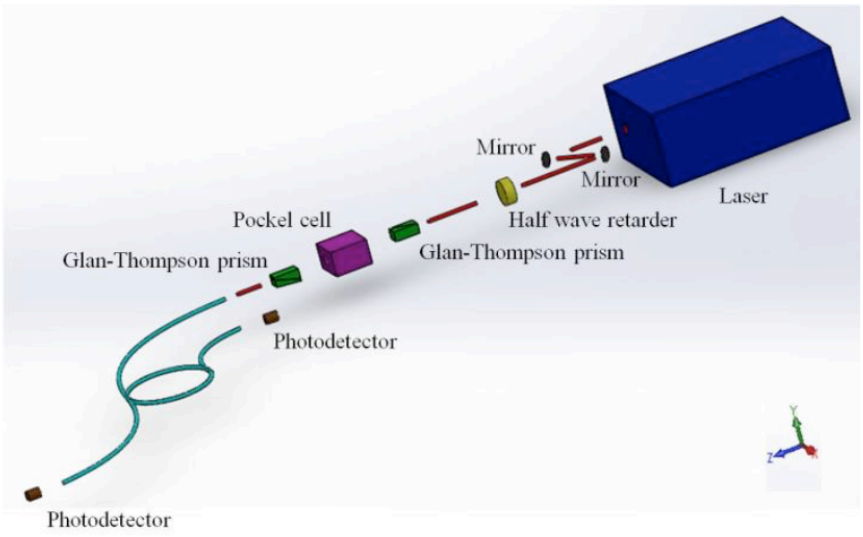


Figure 12. The configuration of the FLRD spectrometer at 800 nm

The averaging number of the oscilloscope used during data accumulation is important for lowering the noise. Ring down time of formed closed loop is measured at different averaging values and the lowest standard deviation is found at 512 average of the oscilloscope (Figure 13). The stability of the RDT of the

closed loop is checked for 30 minutes and standard deviation is found to be less than 1% (Figure 14). The driving voltage of the Pockels cell is another variable parameter and its effect on the noise level is given in Table 3. After optimization of driving voltage level for the close loop (no sample region) FLRD set-up, the lowest noise is obtained when the Pockels cell is driven with 5 kV.

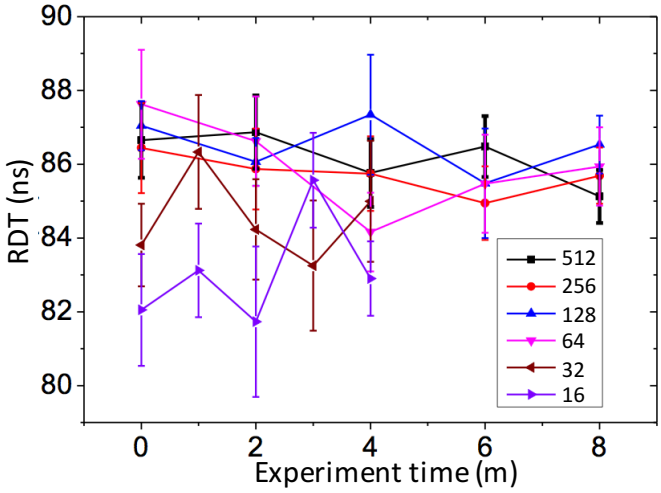


Figure 13. The RDTs' change with average setting of the oscilloscope

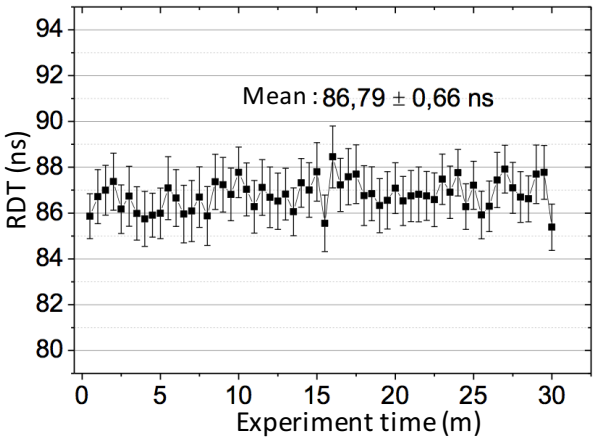


Figure 14. The change of RDT of closed loop during 30 minutes

Table 3. The effect of driving voltage on the RDT of the closed loop

| **Driver voltage (kV)** | **Mean of RDT (ns)** | **Std. deviation (ns)** | **Propagation of errors (ns)** |
|---|---|---|---|
| 4.5 | 87.4 | 0.72 | 2.94 |
| 5 | 86.9 | 0.32 | 2.67 |
| 6 | 86.9 | 0.51 | 2.99 |
| 7 | 86.3 | 0.59 | 2.43 |

The repetition rate of the laser after the Pockels cell modification is another parameter that defines the noise on the RDT. At the same experimental conditions, the lowest standard deviation of RDT is obtained with 200 Hz repetition rate (Figure 15). The trigger time of the oscilloscope is so useful to block noise and its tunability helps to pick the lowest intensity peak clearly. Thus, a study is done to see how it changes standard deviation of measurement. Figure 16 shows that a slight change in standard deviation of measurement is possible. Therefore, in the beginning of the experiment, trigger time which shows the lowest standard deviation of the RDT is found and the rest of the measurements were performed by using the same trigger time.

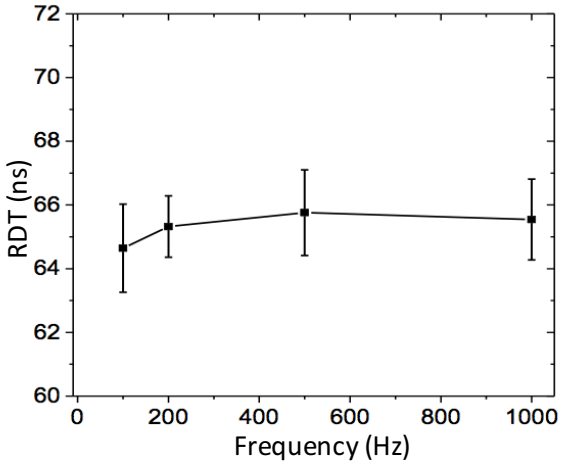


Figure 15. The effect of repetition rate of laser pulse on RDT

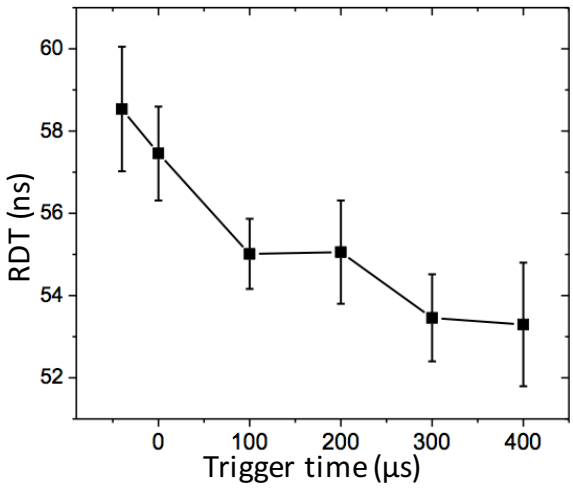


Figure 16. The effect of trigger time on RDT

### 2.3.2. Liquid samples

The performance of the spectrometer with 800 nm wavelength laser is investigated with different samples and by using etched fibers as sensing region (details of etching process are presented in Section 2.4). The optical properties of samples used is listed in Table 4.

The sensing region has the similar configuration as the one used for 1534 nm studies (discussed above in section 2.2.3 and shown in Figure 10) with some important modifications as follows: With the configuration shown in Figure 10, ends of etched fiber region are under both shear and normal stress. Therefore, high attenuation in these ends is observed due to bending. Moreover, high shear stress makes etched fiber handling difficult and it causes fiber being so fragile. Furthermore, free fiber ends cause irreproducible measurement results. Thus, after some initial experiments, ends of etched fiber region are fixed with SU-8 photoresist before etching procedure and the experiments were continued with this configuration. The fixed points are depicted in Figure 17.

The procedure to fix optical fiber to the teflon post is as follows: Wiping fiber out with acetone, pasting ends of fiber with the teflon post by using the

photoresist, baking at 95°C for 20 minutes in furnace, exposing photoresist to 364 nm UV light for 10 minutes and baking at 95°C for 4 minutes in furnace. After this procedure, resistance of photoresist to chemicals such as DMF, DMSO, acetone, ethanol and DI water are tested for more than 2 hours. No color, shape and hardness change were observed with naked eyes.

The three kinds of configurations for sensing unit used in 800 nm liquid sample measurements can be summarized as follows: One of them is that ends of etched fiber not fixed to teflon post with the photoresist and the teflon post is moved to sample beaker for RDT measurement (configuration 1 which is also discussed in 2.2.3), second is that ends of etched fiber not fixed to teflon with photoresist and the teflon post kept at rest while sample moving toward the etched fiber (configuration 2 which is also discussed in 2.2.3) and third is that ends of etched fiber fixed to Teflon post with photoresist and teflon post kept at rest while sample moving toward fiber (configuration 3).

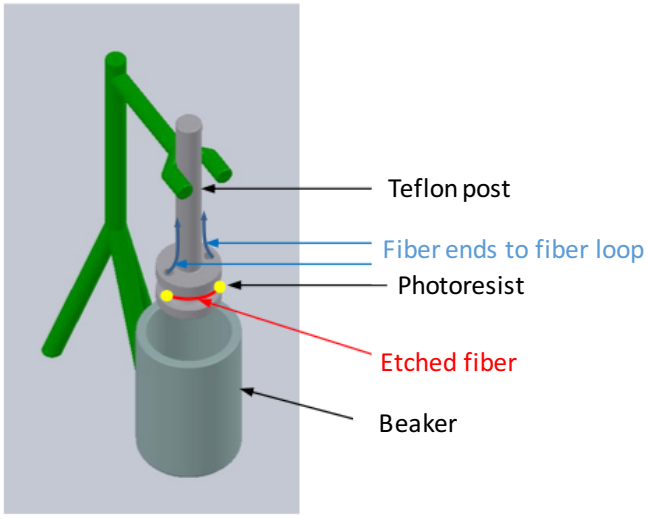


Figure 17. Schematic representation of etched fiber with fixing SU-8 photoresist

Table 4. The optical properties of samples obtained from reference [29]

| **Sample** | **Refractive index @ 1534 nm** | **Ext. coeff. @ 1534 nm** | **Refractive index @ 800 nm** | **Ext. coeff. @ 800 nm** |
|---|---|---|---|---|
| Ethanol | 1.3507 | $6.4353*10^{-5}$ | 1.3565 | $1.6085*10^{-7}$ |
| Acetone | 1.3511* | | 1.3547 | |
| DI water | 1.3183 | $1.0282*10^{-4}$ | 1.3290 | $1.25*10^{-7}$ |
| Benzene | 1.4769 | | 1.4853 | |
| Propanol | 1.3674 | $4.1677*10^{-5}$ | 1.3729 | $9.2768*10^{-8}$ |
| n-Butanol | 1.3859 | | 1.3910 | |
| Toluene | 1.4778 | $1.1567*10^{-6}$ | 1.4864 | $1.5788*10^{-8}$ |
| Octane | 1.39172* | | 1.39449* | |
| Carbon tetrachloride | 1.4483 | | 1.4535 | $3.157*10^{-9}$ |
| Cyclohexane | 1.4162* | | 1.4213 | |
| Hexane | 1,3670* | | 1.3710* | |
| Pentane | 1.3520* | | 1.3546* | |
| Methanol | 1.3173 | | 1.3232 | |
| Acetylene @ 0°C and 1 atm | 1.0005* | | 1.0006* | |
| DMSO | 1.4635* | | 1.4697* | |
| Isopropanol | 1.3667* | | 1.3714* | |

*Value is obtained by using dispersion formula given in reference [29]

The RDT of samples are measured after the integration of the probe (sensor region) into the spectrometer. The high noise level is seen due to integration of the etched fiber so, the Pockels cell driving voltage is set to 6 kV to diminish the noise level as much as possible. Also, repetition rate of the laser is tuned to 1 kHz for the same purpose. The measurements are done after the probe is kept in the sample for 10 minutes after the rinsing of probe with the sample which is measured for 1

minute. Therefore, the contamination at surface of probe is kept at minimum. For each sample, the reported RDT values in the Results section is determined by averaging 10 consecutive measurements performed with 5 second interval.

### 2.3.3. Coating of etched fiber with polymers

The main purpose to coat etched fiber (the procedure for etching optical fiber is discussed in section 2.4) with branched-polyethyleneimine (BPEI) and polystyrene sulfonate (PSS) is testing the performance of the spectrometer with nanometer scale material in thickness. It is a preliminary study for selective sensing before attaching functional groups to much thinner coatings. In this section only procedure for coating of the etched fibers will be mentioned in detail.

For coating studies etched fiber is used without further cleaning. Negative charge is deposited on etched fiber with 0.25 M NaOH treatment for 10 minutes. Next, layer-by-layer deposition of BPEI and PSS are carried out. Two rinsing solutions (both is 0.01 M $NaH_2PO_4$) are used for 2 minutes both to prevent contamination of each polymer solution from previous polymer solution and to stop coating after each polymer coating. These polymers are pH sensitive; therefore, pHs of four solutions are set to 5 before coating. Two piece of square Si lam with almost 1 $cm^2$ are coated in the same beakers of solution with the etched fiber. Therefore, thickness of coating is figured out easily with flat surface of Si lam than with circular surface of optical fiber.

### 2.3.4. Coating of etched fiber with silane

Optical properties of thin materials change dramatically in nanoscale. Thus, these materials can show unique characteristic properties than that of etched optical fiber. Therefore, different optical properties could be detected. For this purpose, coating of etched fiber with smaller molecules such as silane is investigated to see different RDTs. In this study, ends of etched optical fiber are fixed to the teflon post with SU-8 photoresist (details are given in Section 2.3.2). Before the coating process, all equipments such as beaker, tweezers, silicon lam are cleaned with piranha solution for 10 minutes, then rinsed for 1 hour.

The procedure of silane coating onto $SiO_2$ is well established in the literature. [30,31] For that purpose, there are many solvents. The best surface deposition is obtained either with toluene or benzene.[31] Therefore, toluene is used as a solvent for deposition of silane onto etched optical fiber (made up of $SiO_2$) in this study. The experimental part follows as: RDT of toluene is collected with etched fiber for 1 hour before addition of silane into toluene beaker. Then, solution of 1 mM trichlorooctadecylsilane is prepared with toluene. Next, RDT of solution is measured again with the same etched fiber during deposition of silane onto the etched fiber for 1 hour.

## 2.4. Etching optical fiber

There are many ways to observe interaction of laser with sample.[1] One of them is with etched optical fiber. Evanescent field is able to interact strongly with surrounding medium after thickness of fiber decreases to around penetration depth. This decrease in thickness of optical fiber is achieved with etching it with HF acid (Figure 18).

The set-up in Figure 19 is constructed to see interaction strength of evanescent field with surrounding medium. The laser at 808 nm wavelength is used to see radiation loss during etching. The selected portion of optical fiber acrylic is removed with the stripper and it is inserted into 10% (v/v) HF. One end of fiber is directed to the photodetector and the power meter is used to see the laser power which passes through optical fiber. Therefore, the change in the laser power due to radiation loss is monitored easily. The information for the change of optical fiber diameter during etching is collected and presented in Figure 20. The studies with the same concentration of HF solution made at three different days show almost the linear change in the diameter of fiber during etching. However, the etch rate of studies labeled as etching 4 and 5 are different than others. It is believed that there is local concentration difference in the etchants. With the same study, the radiation loss increasing with decreasing diameter of optical fiber can be seen in Figure 21. In this experiment, the longer etched region of fiber is supposed to show

much more radiation loss. However, the expected result in this experiment is not achieved because of unknown reason.

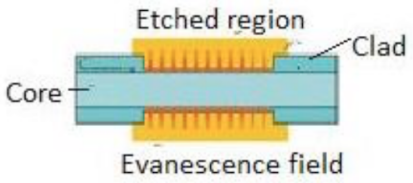


Figure 18. The evanescent wave across the etched optical fiber [1]

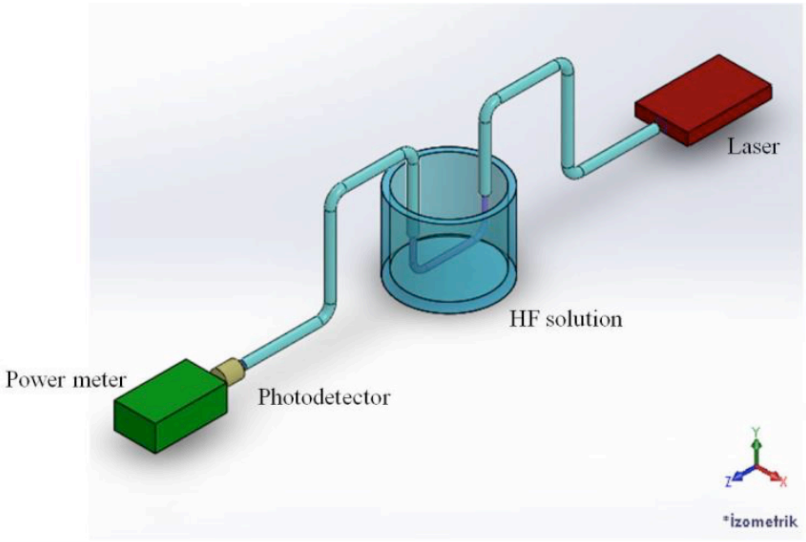


Figure 19. The set-up for etching optical fiber

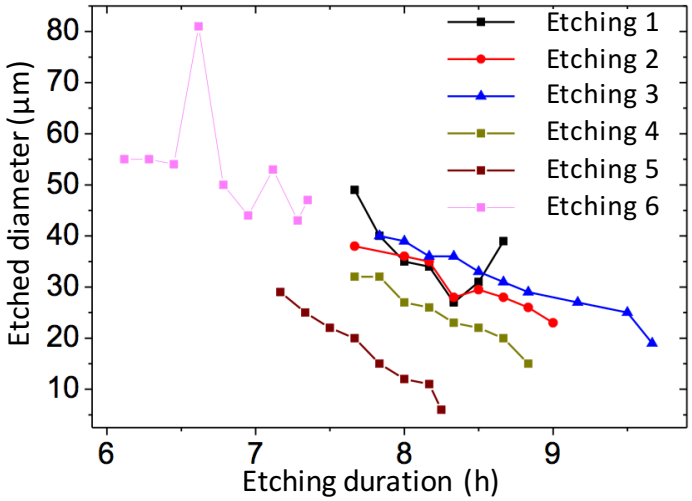


Figure 20. The change of optical fiber diameter during etching

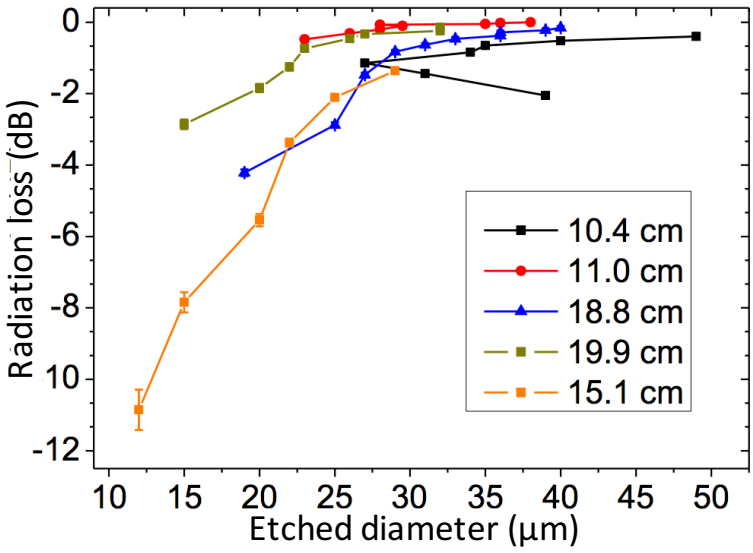


Figure 21. The radiation loss change with the etched fiber diameter

## 2.5. Splicing SM fiber to MOF

Splicing of single mode (SM) fiber to microstructured optical fiber (MOF) having 5 µm inner (hollow core) and 125 µm outer diameters (Figure 22) is tried while measuring transmission loss with the laser at 642 nm wavelength having 21 mW output power. Splice parameters at this wavelength are used for the FLRD set-

up at 800 nm because literature shows that wavelength of laser has no much impact on measurement of splice loss.[32] Therefore, parameters of splicing obtained with 642 nm wavelength laser may be used for laser having 800 nm wavelength.

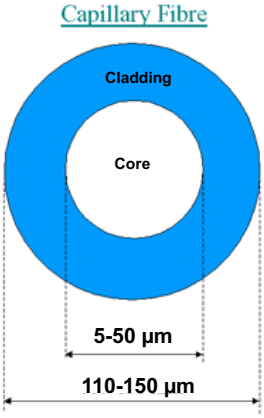


Figure 22. Geometrical structure of capillary fiber

In this experiment, the equipment used is listed in Table 5. Some of splice parameters are fixed whereas others are variable which are given in Table 6. The parameters which provide the least splicing loss are found by trial and error while keeping the length of MOF almost constant. At each parameter survey, three trials are done for reproducibility of the measurements. Transmitted power through MOF for parameter survey is measured after cleaving fiber end(s) and subsequently wiping fibers with methanol.

Table 5. The equipment for splicing

| **Equipment** | **Model/ Specification** |
|---|---|
| Arc fusion splicer | Fujikura FSM-60S |
| Single mode fiber for 800 nm wavelength | 4.4 µm core and 125 µm cladding diameters |
| Microstructured optical fiber (MOF) | 1. 5 µm core and 125 µm cladding diameters<br>2. 50 µm core and 125 µm cladding diameters<br>3. 2 µm core and 150 µm cladding diameters<br>4. 50 µm core and 192 µm cladding diameters |
| Multichannel diode laser | 21 mW power at 642 nm wavelength |
| Powermeter | Thorlabs |
| Cleaver | Fujikura CT-32 |

Table 6. Parameters of the arc fusion splicer

| **Constant splicing parameters** | | **Variable splicing parameters** | |
|---|---|---|---|
| Proof test | OFF | Gapset position | 0-30 µm |
| Cleaning arc time | 150 ms | Prefuse arc time | 50-70 ms |
| Gap | 15 µm | Overlap | 10-25 µm |
| Prefuse power | Standard | Arc1 time | 600-900 ms |
| Arc1 power | Standard | | |

First, gapset position which defines the distance between joint point and arc discharger was examined for joining of single mode fiber to MOF while measuring optical transmission loss. Figure 23 presents that the lowest loss was seen when

gapset position is 15 µm. This 15 µm distance means that arc discharging takes place 15 µm from joint toward single mode fiber. Secondly, prefuse time was studied and 60 ms showed the lowest mean of splicing loss (Figure 24). However, cleavege angle of MOF could not be controlled precisely with the cleaver which is available in the lab and it is important for low loss splicing. Therefore, 50 ms prefuse time is prefered for further studies because, it supplies the lowest loss. Arc1 time which is the duration of arc for butt joint was also studied and 700 ms gave the best results as can be seen in Figure 25. The arc1 time was not enough to combine two fibers when it is 200, 300, and 400 ms. Some unsuccessful splicing results with these arc1 time values are shown Figure 26. Overlap of fibers during arc discharging is another parameter which is easily set. The study of this parameter indicated that 20 µm is the best value for the lowest splicing loss (Figure 27).

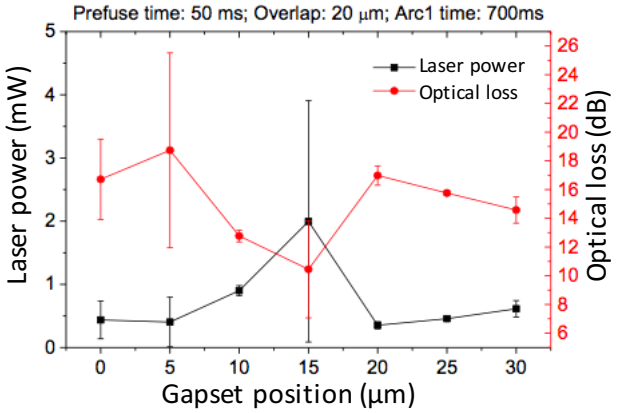


Figure 23. The effect of gapset position on butt joint of single mode fiber to 5 µm inner diameter MOF (Constant parameters are specified on the top of figure)

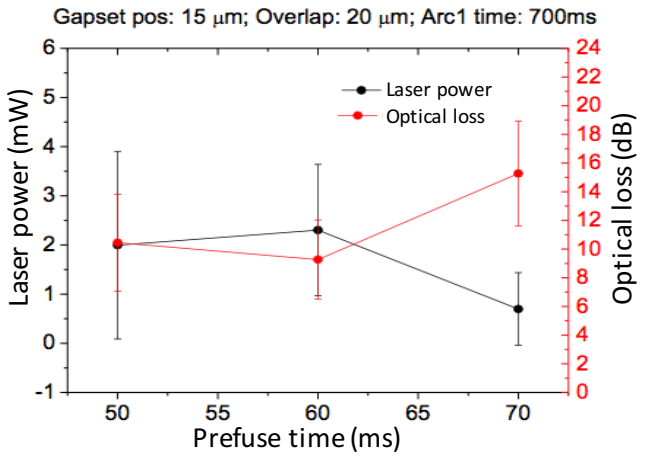


Figure 24. The effect of prefuse time on butt joint of single mode fiber to 5 μm inner diameter MOF (Constant parameters are specified on the top of figure)

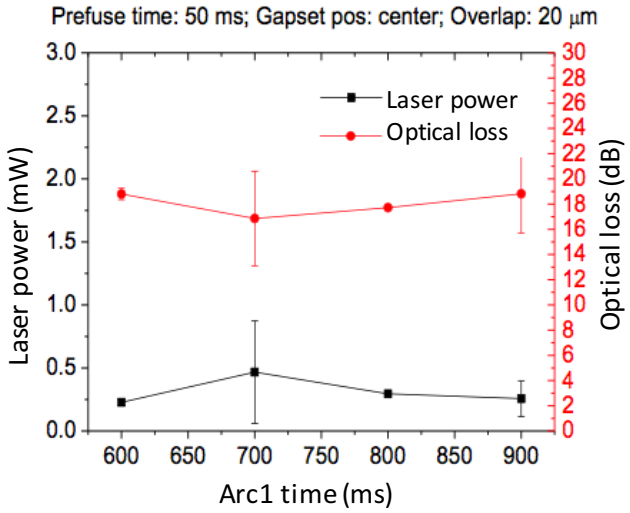


Figure 25. The effect of arc1 time on butt joint of single mode fiber to 5 μm inner diameter MOF (Constant parameters are specified on the top of figure)

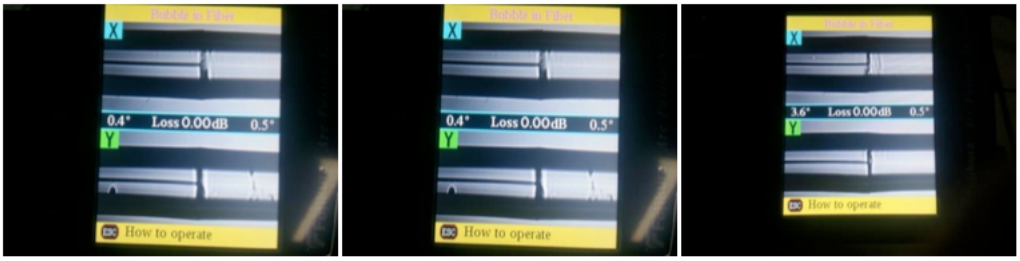


Figure 26. The photographs of splicing with arc1 time 200, 300, and 400 ms

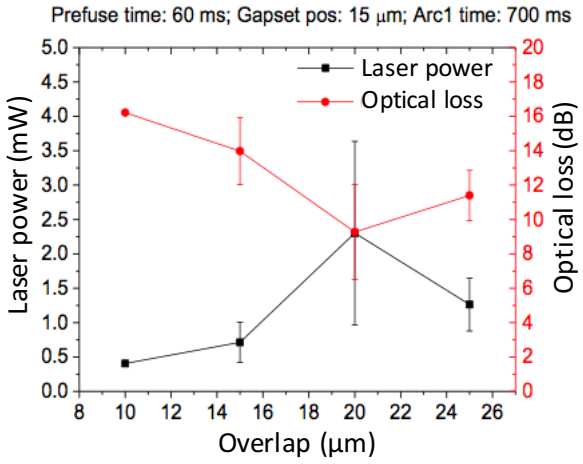


Figure 27. The effect of fibers overlap during arc discharge for butt joint of single mode fiber to 5 μm inner diameter MOF (Constant parameters are specified on the top of figure)

As a result, the found arc parameters for splicing the single mode fiber to 5 μm inner core MOF are 15 μm "gapset position", 50 ms "presfuse time", 700 ms "arc1 time", and 20 μm "overlap". With these parameters, conic structure roughly 150 μm from the splicing point toward MOF is formed (Figure 28). Moreover, results of splicing parameter studies have high standard deviations and these do not secure reproducibility. Furthermore, cleave angle of fibers could not be controlled with high accuracy and high precision, so it is another obstacle for reproducibility.

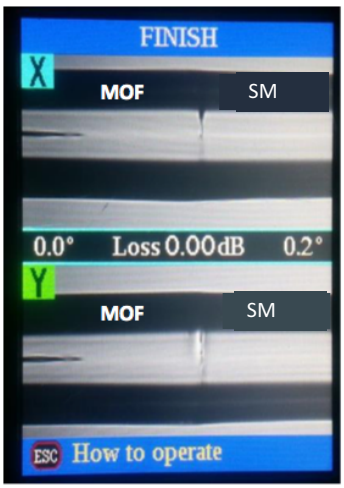


Figure 28. The photograph of splice of single mode fiber to 5 μm inner diameter MOF

The acrylic coating (buffer) length of MOF changes amount of light guided through MOF. Thus, the effect of coating length is studied while decreasing length of coating of 8.3 cm long MOF. Figure 29 shows that power of guided laser increases with decreasing length of MOF coating. Also, length of MOF changes amount of transmitted light through MOF as seen in Figure 30. In these studies, the length of acrylic coating for splicing studies 1&2 was kept 2 cm shorter than length of MOF. For splicing study 3, length of coating was kept fixed at 1.5 cm and MOF length is decreased step-by-step. In Figure 30 transmitted power through MOF is higher for splicing study 3 than for spicing studies 1&2 because MOF in the study 3 has shorter buffer length than others. Moreover, amount of guided light rises exponentially with decreasing length of MOF.

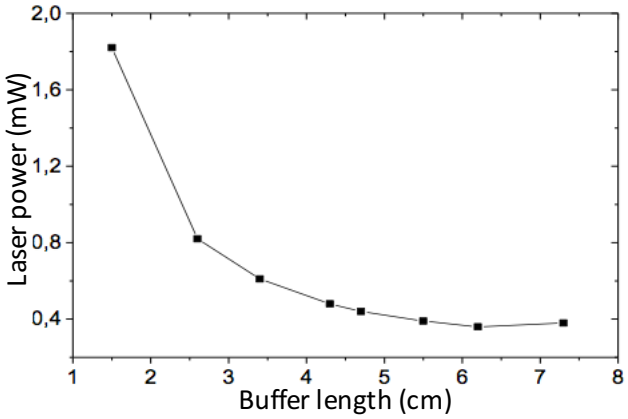


Figure 29. The change of transmitted power through MOF when length of MOF coating decreases

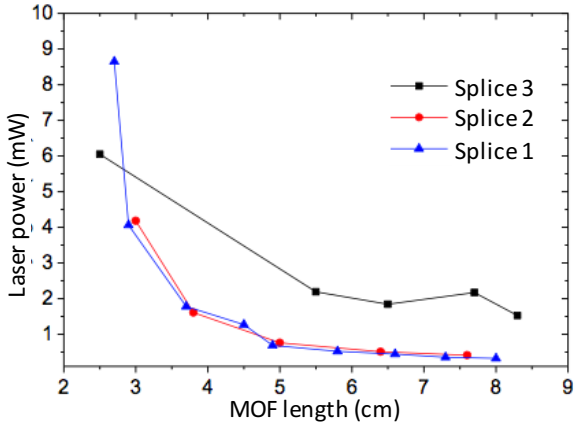


Figure 30. The change of transmitted power through MOF when length of MOF decreases

With the same splicing parameters, similar experiment is carried out for 50 μm (hollow) core diameter MOF (Figure 22). Figure 31 shows that amount of light guided through MOF of 50 μm inner core diameter rises with decreasing length of MOF. Moreover, transmitted light power with this MOF is less than that for MOF of 5 μm inner core diameter (see Figure 30 & Figure 31). With 5 μm inner core diameter MOF, sample cell is constructed after splicing both ends of fiber with single mode fiber as shown in Figure 32. As it is depicted in the figure, output power of 642 nm wavelength laser is measured at three points as before splicing of

1st MOF, after splicing of 1st MOF and after splicing of 2nd MOF with single mode fiber. On the other hand, in this study, it is regarded that optical loss of single mode fiber after measurement point 3 has no contribution to total loss. The powers for these three measurement points are listed in Table 7 and it is believed that with this MOF cell, 1.8 mW transmitted power at trial 3 is enough to see sufficient round trip peak number for sensitive RDT measurement.

Table 7. The loss measurement for the sample cell constructed with 5 μm inner diameter MOF

| | **d, MOF length, [buffer length] (cm)** | **Laser power at meas. point 1 (mW)** | **Loss between 1 &2 (dB)** | **Loss between 2 &3 (dB)** | **Laser power at meas. point 3 (mW)** |
|---|---|---|---|---|---|
| Trial 1 | 4.9 [2.9] | 21 | 14.6 | 2.36 | 0.4 |
| Trial 2 | 2.9 [0.9] | 21 | 6.46 | 6.84 | 0.84 |
| Trial 3 | 2.7 [0] | 21 | 3.85 | 6.84 | 1.8 |

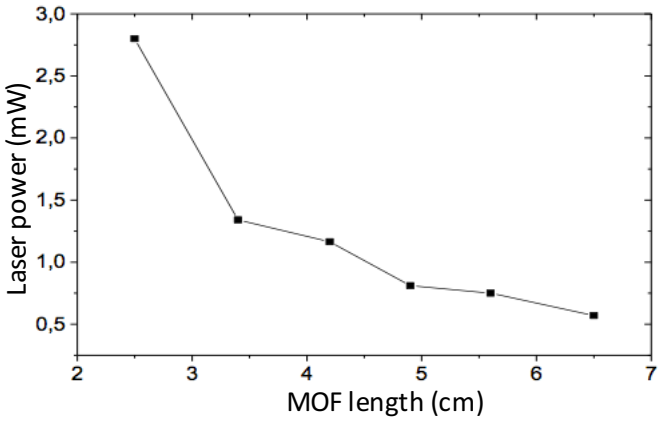


Figure 31. The change of transmission power for MOF of 50 μm inner diameter through MOF with decreasing of MOF length

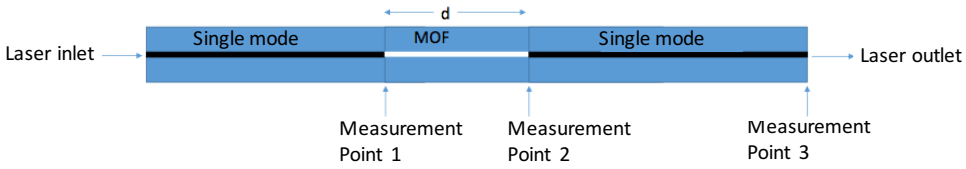


Figure 32. The sample cell constructed with 5 μm inner diameter MOF

# CHAPTER 3

# RESULTS AND DISCUSSIONS

Here, all of the results obtained with three spectrometers using two laser sources (at 800 and 1534 nm) are presented. Firstly, the spectrometer at 1534 nm for sensing gas is tested for stability. Then, various concentrations of acetylene in nitrogen is studied at different pressure values. Next, detection limit of this spectrometer is improved with a mathematical method "reference correction". Afterward, the spectrometer at 1534 nm for liquid samples is reported and achievements based on evanescent field interaction is discussed. Then, the results with the spectrometer at 800 nm for sensing of liquid sample are discussed and important findings are mentioned. Finally, results obtained in each section are compared with literature.

## 3.1. Gas sample measurement with direct interaction at 1534 nm[1]*

Here, the limitation, stability, sensitivity, and detection limit of the spectrometer constructed with 1534 nm wavelength laser is mentioned in detail (see Section 2.2.2 for experimental detail). Effects of pressure and concentration on RDT of acetylene are discussed and inherent behaviour of the spectrometer is discussed. Lastly, results are compared with literature and achievements are highlighted.

For detection of acetylene, $N_2$ gas is used as a reference since $N_2$ does not have a significant absorption at 1534 nm. The $N_2$ RDTs at 25 psia are measured for an extended period at three different days to check the system stability and day-to-

[1]*The results discussed in this section were published in the article.[36]

day variation. Though there are some daily variations, RDTs of $N_2$ are quite stable on each day as shown in Figure 33. The relative standard deviation is less than 0.043% at each day, and is better than the ones reported in the literature.[21,23,33] The observed daily variations in the RDT are in part due to the environmental changes.

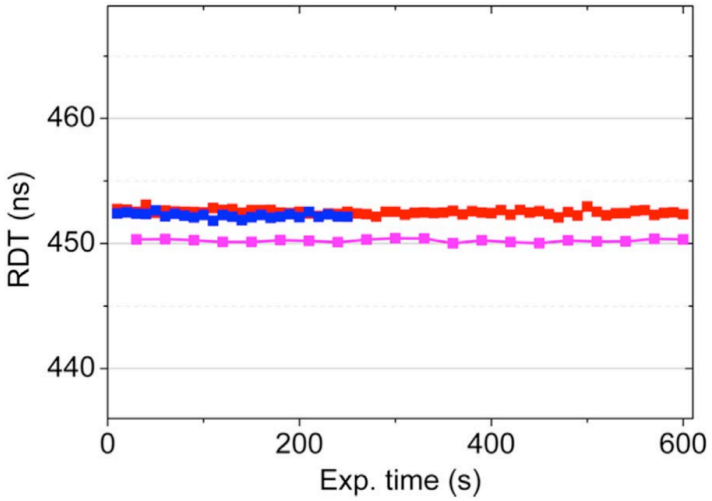


Figure 33. Ring down time of N2at 25 psia over time at three different days. The relative standard deviation is less than 0.043% at each day.

The peak points of the pulse train collected for acetylene concentrations between 0.1% and 100% at 25 psia are given in Figure 31 after the background correction. Table 7 presents the RDTs and average loss at each round trip with their errors. The faster decay rate is clearly seen both in the figure and in Table 8 as the concentration increases to 100%. There is a significant decrease in the number of pulses in the pulse train as the concentration increases due to absorption of acetylene at 1534 nm. Even though the exponential decay of the peak amplitude in pure acetylene is much stronger and results a significant number of peak losses in the pulse train, the standard deviation is quite close to the other concentrations. Thus, a lower number of peak points in the decay fit does not have a significant impact on the measurement. Another important observation is that the difference in RDTs of 0.1% and 1% acetylene is larger than their standard errors, hence, even at

25 psia it is possible to distinguish concentration lower than 1% (inset in Figure 34). At higher pressures, this difference becomes much more clear.

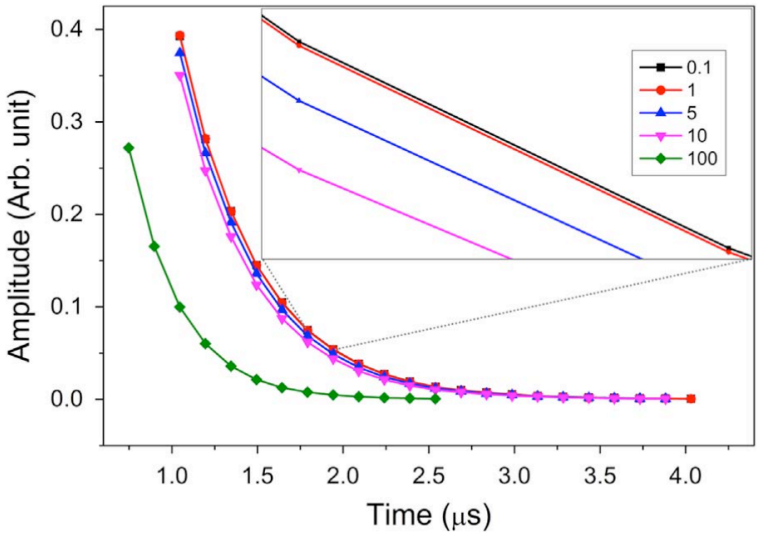


Figure 34. Peak intensities of the pulses in the ring for 0.1%, 1%, 5%, 10%, and 100% acetylene/nitrogen mixture at 25 psia.

Table 8. RDT of the samples at 25 psia and their average loss at each round trip.

| % C2H2 | RDT(ns) | σ (ns) | Loss (dB) | σ (dB) |
|---|---|---|---|---|
| 0.1 | 449.6 | 0.6 | 1.439 | 0.002 |
| 1 | 447.8 | 0.5 | 1.445 | 0.002 |
| 5 | 440.0 | 0.6 | 1.471 | 0.002 |
| 10 | 429.8 | 0.5 | 1.506 | 0.002 |
| 100 | 296.5 | 0.6 | 2.183 | 0.005 |

The RDTs of various concentrations of acetylene and pure nitrogen on the set total pressure are given in Figure 35. As expected RDT of any concentration decreases with increasing pressure since the acetylene concentration (or partial pressure) increases within the fixed volume. With increasing pressure, the

acetylene absorption bands are expected to broaden. However, in the pressure range we work this broadening will not be greater than 0.01 nm (at 65 psia), which is much smaller than the band width of our laser (6 nm). Hence pressure broadening is not expected to have significant (if any) effect on the observed RDTs. At low pressure settings it was difficult to observe differences in the RDT of $N_2$ and 0.1% mixture as shown in the inset of Figure 35. However, as the pressure is increased, especially beyond 45 psia, the difference in RDTs becomes much larger than the standard errors. Thus, it becomes possible to quantify 0.1% acetylene in $N_2$. The results also indicate that lower than 0.1% concentrations could also be detected at higher pressures. Such a small difference between the RDTs of $N_2$ and 0.1% acetylene in $N_2$ led us to do multiple averaging and reference correction for clear discrimination of acetylene at low concentrations. As shown in Figure 35, as the pressure of the mixtures increases the differences in the RDTs increase significantly. In fact, there appears to be an exponential dependence on the pressure.

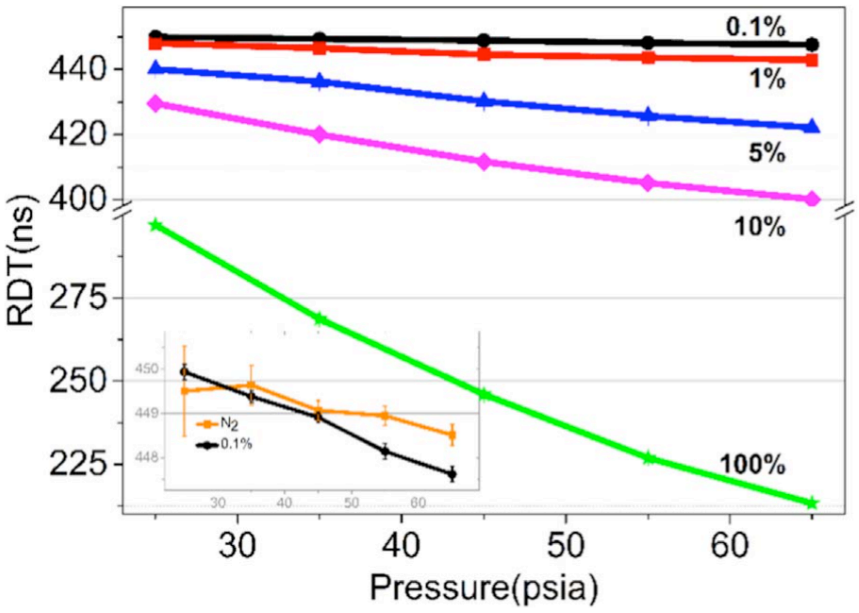


Figure 35. The ring down time of acetylene and nitrogen mixtures at different pressures. Inset shows RDTs of the reference $N_2$ and 0.1% acetylene.

Though the reference correction is not really necessary except for 0.1% acetylene, it is performed on all the data sets. Nitrogen gas is measured at each pressure as a reference that includes the response of the system in the absence of any absorbent species before measuring any samples. This measurement is important since the intrinsic losses of the spectrometer changes slightly due to the environmental conditions. Moreover, RDT of $N_2$ (which is expected to increase very slightly due to increasing refractive index with pressure[34]) decreases slightly possibly due to slight motion of the optical components at higher pressures.

Absorbance of analyte at pressures ranging from 0.02 psia to 65 psia were calculated by the equations given equations 10-to-12. Intrinsic system contributions to the analyte measurements were determined by the reference $N_2$ measurements ($A_{sys}$, Equation 10). Then its contributions were subtracted from the sample measurement ($A_{C2H2+sys}$, Equation 11) and the analyte absorbance ($A_{C2H2}$, Equation 12) was determined. The round trip time ($t_r$) of 145.9 ns was calculated from the experimental data of $N_2$ measurements.

$$A_{sys} = -log_{10}\left(I/I_0\right) = \left(t_r/\tau_{N2}\right) * log_{10}(e) \qquad \text{Equation 10}$$

$$A_{C2H2+sys} = -log_{10}\left(I/I_0\right) = \left(t_r/\tau_{C2H2+N2}\right) * log_{10}(e) \qquad \text{Equation 11}$$

$$A_{C2H2} = A_{C2H2+sys} - A_{sys} \qquad \text{Equation 12}$$

Difference between RDTs of the mixture and that of the reference nitrogen at each pressure is correlated with the absorbance of the acetylene amount. Subtraction of reference nitrogen eliminates the effect of the optical components' possible movements at high pressures and slight day-by-day variations. Then, absorbance of acetylene at the corresponding partial pressures were calculated from the differences in RDTs and all the data is merged into a single plot of absorbance as a function of acetylene partial pressure in the mixture as shown in Figure 36. As expected, there is a clear linear dependence on the partial pressure of acetylene. As the concentration is increased, a slight deviation from linearity is

observed at high concentration. The deviation from linearity at high pressures might be due to increased analyte-analyte interaction, change in refractive index, or higher scattering rate as pressure increases. RDT vs pressure of the individual mixtures given in Figure 35 show similar deviation as the pressure is increased, especially for 10% mixture and the pure acetylene sample. The observed deviations may also be associated with the instrument/spectrometer nonlinear response if it is not corrected very well with the reference measurement as the pressure increases.

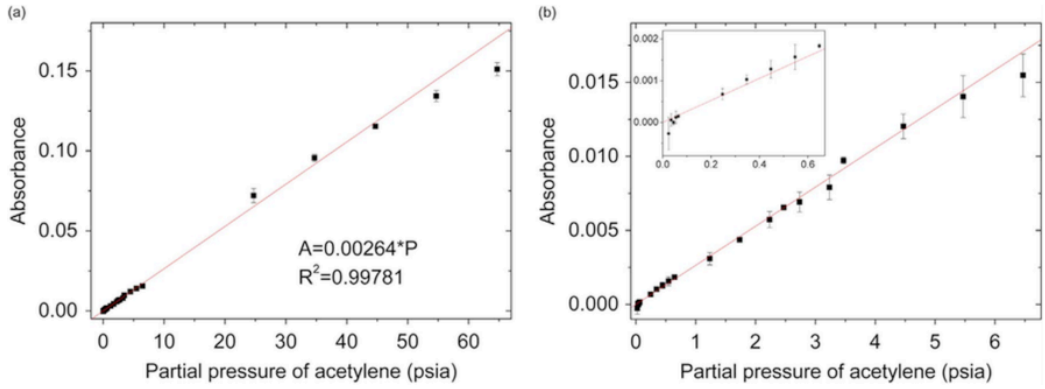


Figure 36. Absorbance of the acetylene with respect to partial pressure of acetylene in $N_2$, (a) for all the set partial pressures and (b) up to 6.7 psia. The inset presents the data up to 0.67 psia.

Our setup yields the best detection performance at 65 psia total pressure, as can be seen in Figure 35. With the calibration line shown in Figure 36, the limit of detection is calculated as 0.1% at this total pressure value (65 psia) with an absorbance sensitivity of 378 psia (that corresponds to a measurement sensitivity of 0.0026 $psia^{-1}$, see APPENDIX C) [35]. This result indicates that we can successfully detect acetylene concentration down to 0.1% (v/v) despite our simple configuration, intra-cavity free space set-up and use of commercially available equipment. The spectrometer brings some advantages compared to the ones reported in the literature. The presented setup is simpler and has better detection limit than the one reported by Zhang et al.[20] The sensitivity of our setup is similar

to the one reported by Zhao et al. [21,23]; however, a basic advantage of this spectrometer is its simplicity, short loop length, and elimination of FBG or EDFA in the cavity. These advantages may suggest a more compact and low cost spectrometer in future for detection of chemicals with fiber loop ring down spectrometers.

### 3.2. Evanescent field based interaction at 1534 nm

In this section, results obtained by using etched fibers as sensing region with 1534 nm laser for liquid samples will be discussed (see section 2.2.3 for experimental details). Speed of our detection technique (ie. response time) is also deliberated on and compared with those of similar systems reported the literature. Lastly, results are compared with literature and contributions to literature are highlighted.

First measurements show that RDTs of ethanol, DI water and DMSO are almost constant during experiments (Figure 37). Moreover, 1 data point is enough to measure RDT of ethanol as seen in Figure 37.A. Stable RDT of acetone, DI water, DMF, and DMSO are obtained after 600, 400, 500 and 600 seconds respectively as shown in Figure 37.B&C.

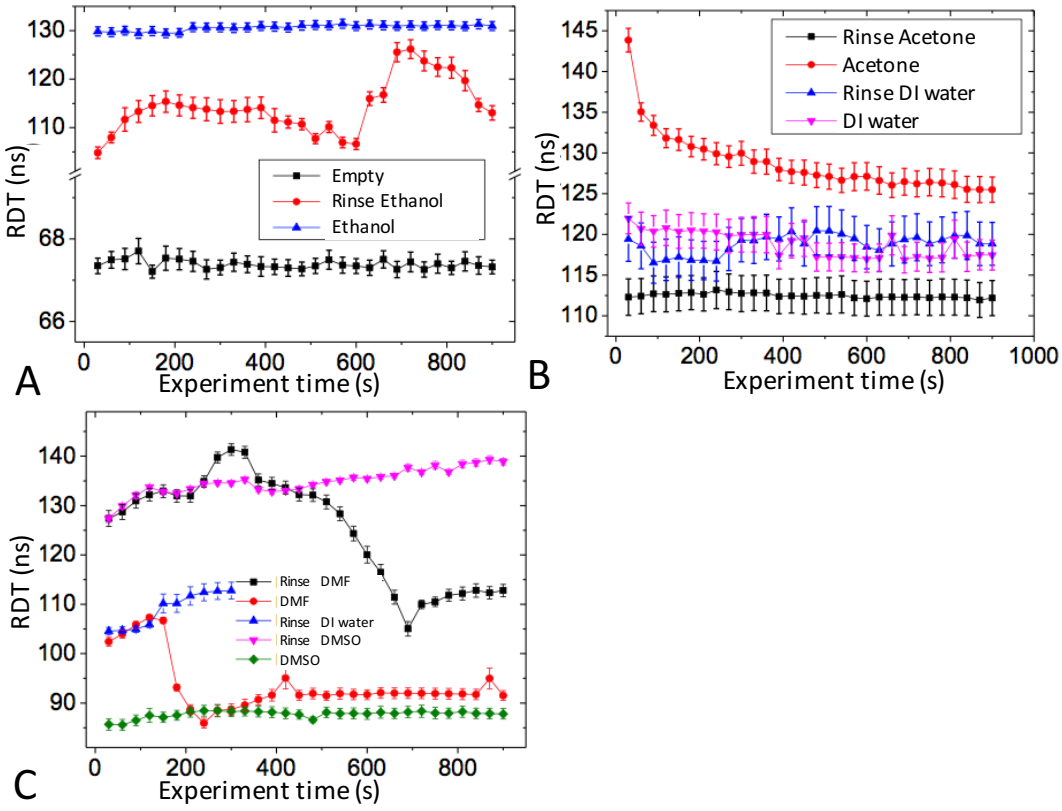


Figure 37. RDTs of different sample during the experiment

Iterative measurements of ethanol while keeping the probe at rest yield the same RDT values as shown in Figure 38. This confirms that etched optical fiber does not move in sample and it is believed that there is no change in RDT due to slight movement of either etched fiber or sample. However, this assumption is valid for this etched fiber specification. Because, higher penetration depth of evanescent field is seen with thinner optical fibers, so field may be so sensitive to slight change in the environment of measurement. Figure 39 presents RDT measurements of different samples performed by using the same etched fiber as sensing unit. After 600 seconds all the samples show stable RDTs during experiment and distinct/characteristic RDT values due to their different optical characteristics. It is important to note that difference in RDT for each sample are strongly correlated with geometrical parameters of the etched fiber. Even though all measurements were performed with the same etched fibers, for ethanol the RDT

values in Figure 37.A, Figure 38, and Figure 39 are different. The reason is thought as contamination of etched fiber is not kept away after it is rinsed with ethanol and acetone.

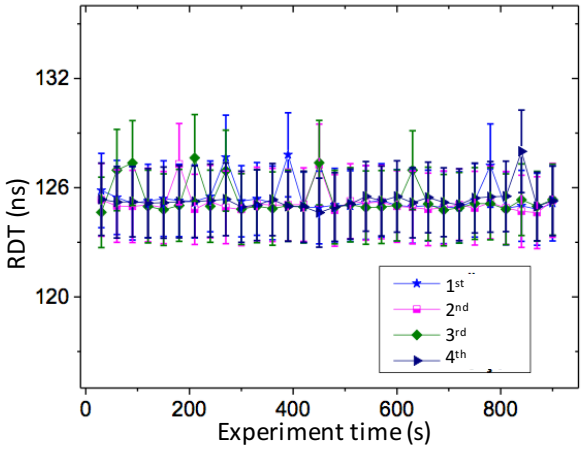


Figure 38. The testing repeatability of measurement with ethanol.

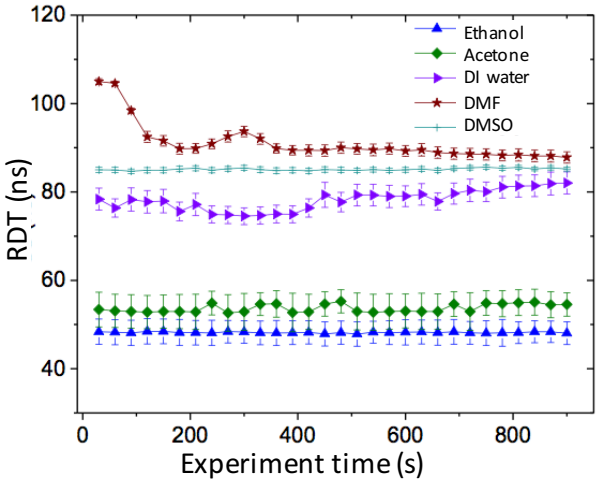


Figure 39. RDTs of ethanol, acetone, DI water, DMF, and DMSO (Results of rinsing step are not presented in this figure)

As a result of these studies, after the integration of etched optical fiber to FLRD spectrometer with 1534 nm wavelength laser, ethanol shows stable RDTs in time for three measurements in three different days. Moreover, one single RDT measurement, which takes 5 second, is enough for sensing, detection and

characterization of ethanol. In other words, fast detection of ethanol is possible with FLRD using evanescent field interaction. Besides, acetone, DMF and DMSO show quite stable RDTs for 30 minutes in two measurements and sensing/detection of these chemicals may be performed within 30 minutes. Moreover, there is no similar spectrometer for sensing of acetone, DMSO, DMF, and ethanol in literature. Some achievements by using laser around 1515 nm were reported for sensing of DI water in literature. The sensor regions in these studies have almost similar geometrical parameters like that in this study.[25,26,27,12] There are a few studies which perform fast response for RDT measurements as Hearth et al (<1 s))[26] and Alali et al(≈1 s)[10] did. The fastest response of the spectrometer in this section is 5 seconds and it is achieved with ethanol. Fast detection of ethanol with FLRD technique does not exist in literature and this study reveals possibility of fast detection of ethanol concentration.

### 3.3. Evanescent field based interaction at 800 nm

In this section, results obtained by using etched fibers as sensing region with 800 nm laser for liquid samples is mentioned (see section 2.3 for experimental details of liquid samples and coatings of etched fiber). The repeatability of RDT measurements is revealed by using ethanol and acetone as samples. Different optical properties of samples such as toluene, cyclohexane, dodecane, DMSO, DMF are shown with this spectrometer based upon difference in RDTs. Then, results of food dyes as absorber in this wavelength are discussed. Moreover, the best achievements for coating of etched fiber with polymer film are mentioned. Lastly, results are compared with literature and contributions to literature are highlighted.

The FLRD set-up is constructed with optoelectronic, electro-optic and optic items at first (see section 2.3 for details). This configuration is unique in literature and there is no similar configuration and detection/sensing at around this wavelength as far as we know. After the set-up constructed with Pockels cell, performance of the spectrometer is tested with chemicals and ultrathin coatings. To this end we first tried to detect/distinguish different solvents. Then we performed

studies for identifying the best solvent for silane film growth on etched fibers. Next we tried to detect/distinguish different color dyes based on their absorption at 800 nm. Finally, we studied polymer bilayer coated change in the RDT values with changing polymer film thickness.

### 3.3.1. Chemicals

Initial experiments started with ethanol, acetone, and DI water as samples by using configuration 1 (discussed in Section 2.3.2). The different RDT values for acetone whose refractive index is 1.3547 and for air (indicated as empty in the figures) whose refractive index is roughly 1 can be seen in Figure 40.A. In this experiment, 5 ns RDT difference corresponds to 0.3537 refractive index unit. The average RDT for ethanol and DI water are measured as 79 ns and 76 ns respectively (Figure 40.B). This, almost 3 ns RDT difference, corresponds to 0.0275 refractive index unit. The average RDT for acetone and DI water are measured as 83 ns and 75 ns respectively and these results correspond to 0.0257 refractive index unit (Figure 40.C). Lastly, RDT difference of acetone and ethanol, instead of DI water, is studied to check the performance of the spectrometer due to difficulty of cleaning DI water. Finally, the clear discrimination of RDT of acetone and ethanol is obtained with 0.0018 refractive index unit difference (Figure 40.D). However, there is no linear comparison between refractive index difference and RDT difference. Furthermore, this type of comparison is highly affected with the specification of probe, thus; detection/characterization of measurements for sample should be done with the specific etched fiber.

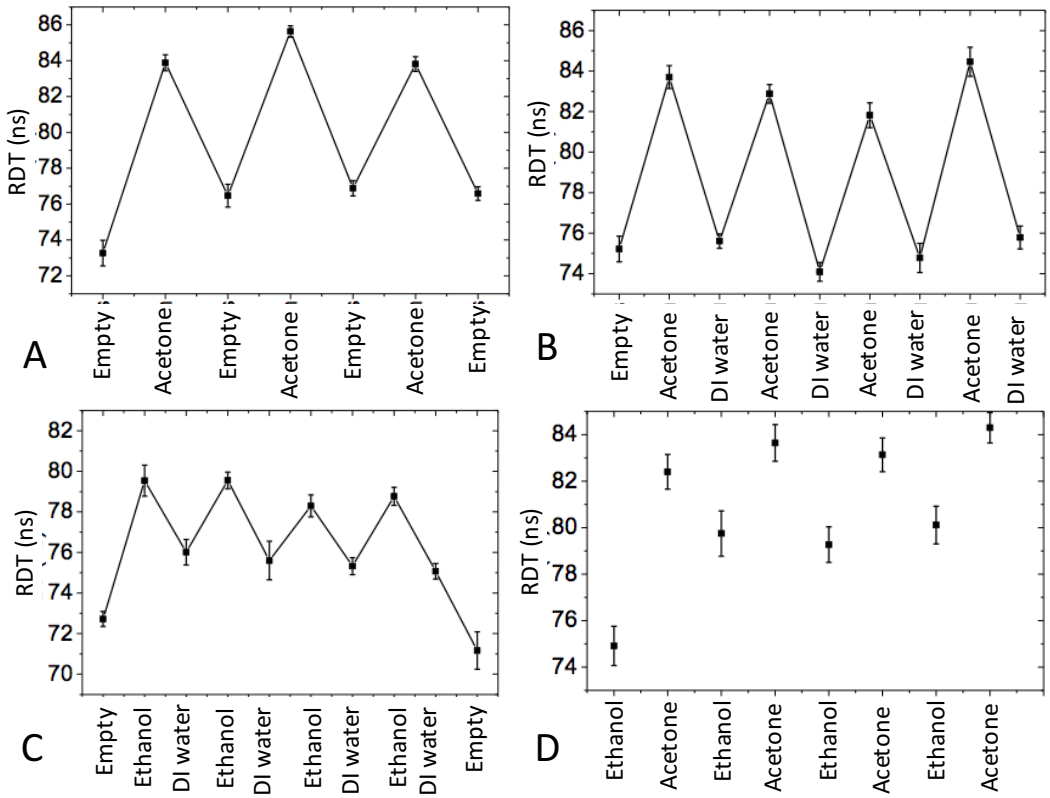


Figure 40. The sensing of various sample with the etched fiber with first probe configuration (The geometrical parameters of etched fibers: A,B&C) 36 μm diameter and 7.0 cm length, D) 35 μm diameter and 5.0 cm length )

A sequence of experiment while keeping the fiber fixed and moving sample toward the fiber (configuration 2, see Section 2.3.2) is done to be sure that there is no contribution to RDT whether etched fiber moves in sample. The results show that RDTs of ethanol are quite stable within 5 trials after RDTs of ethanol are measured consecutively (Figure 41.A). Furthermore, the similar behavior is observed for acetone with the same procedure (Figure 41.B). The clear observation for the stability can be seen in Figure 41.C where the average of 5 trials are plotted for both ethanol and acetone. After these studies, performance of the spectrometer is compared based upon difference of RDTs between acetone and ethanol. First measurement with the same etched fiber shows that there is almost constant difference between RDTs of acetone and ethanol (Figure 41.D).

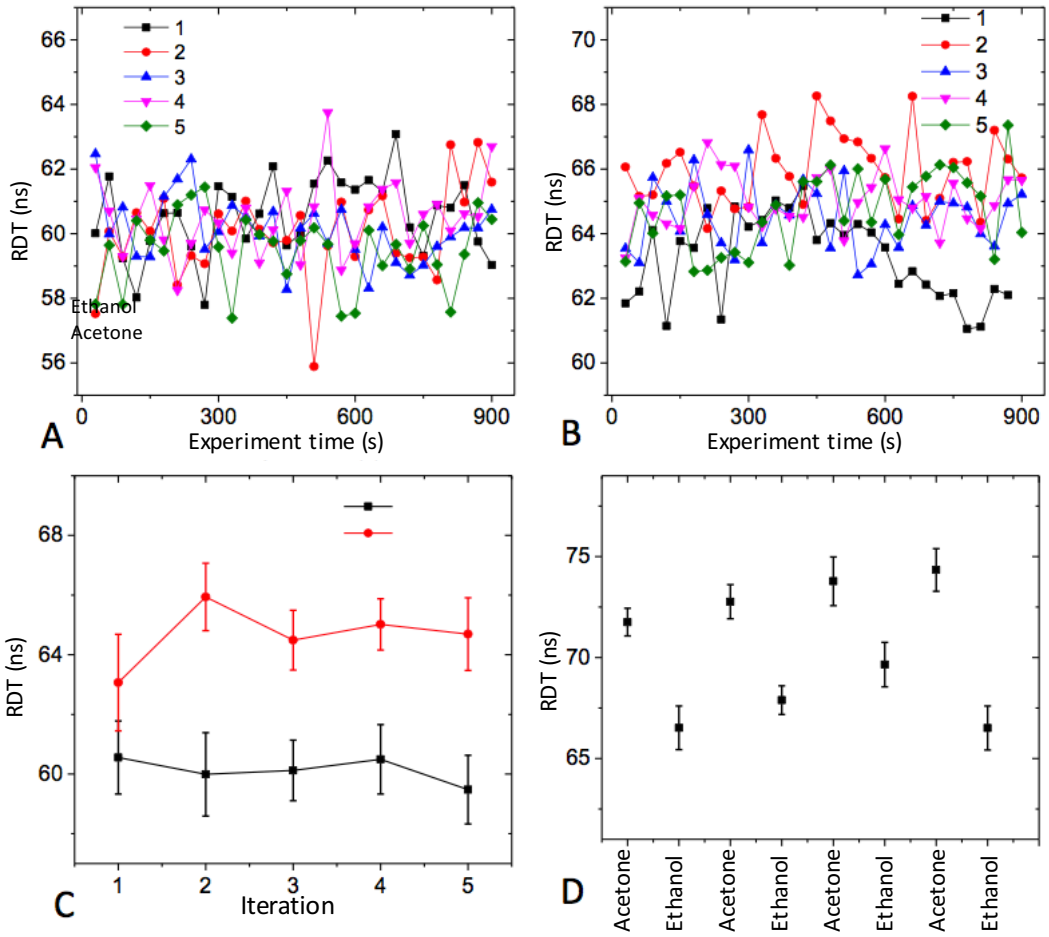


Figure 41. The stability checks of ethanol and acetone second probe configuration (All samples are sensed with 35 µm diameter and 9.8 cm length etched fiber)

Other chemicals are also used to detect refractive index difference with this spectrometer. DMSO, DMF, and DI water have different RDTs with etched fiber 35 µm diameter and 9.8 cm length as can be seen in Figure 42.A. However, DI water, n-Butanol, and Isopropanol show similar signal with the same etched fiber (Figure 42.B). With the etched fiber 28 µm diameter and 6.8 cm length, difference of RDTs of DMSO and DMF rises compared to the values reported in Figure 42.A. However, DMF, nButanol and isopropanol have similar RDTs as in Figure 42.B and Figure 42.C.

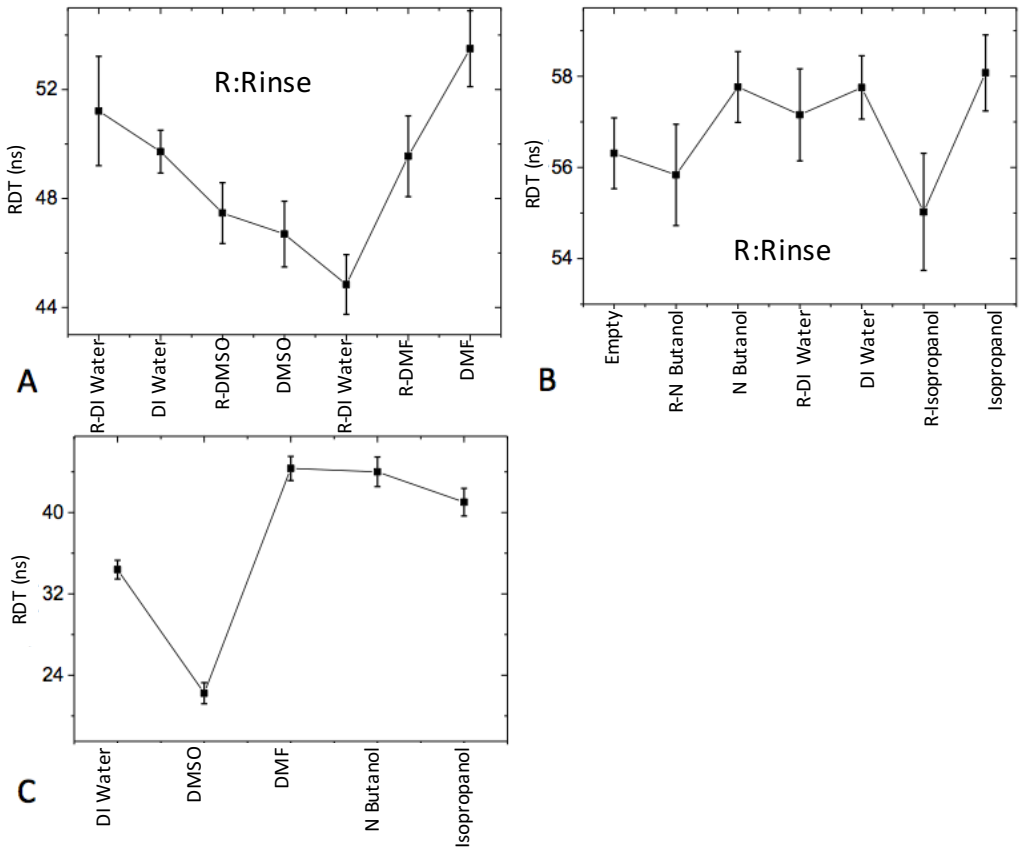


Figure 42. The RDT of various sample second probe configuration. (All samples are sensed with 35 μm diameter and 9.8 cm length etched fiber)

We also performed measurements for determining the best solvent for silane coating with configuration 3 (see Section 2.3.2 for detail). Most commonly used solvent for this purpose in the literature is toluene. However, RDTs of toluene are measured as zero because refractive index of toluene is higher than fiber (Figure 43.A). Thus, there is no internal reflection at the fiber/solvent interface so, radiation mode is seen instead of guiding mode. Higher difference in RDTs of toluene and ethanol can be achieved by using a thinner etched fiber (Figure 43.B). Cyclohexane, n-octane, and decane are chosen as a solvent to deposit silane onto the etched fiber instead of toluene. RDTs of these solvents are compared in order to see non-zero RDT with ethanol as a reference (Figure 44). The difference of dodecane with respect to ethanol in RDT is not stable in all

measurements (Figure 44.C). Fortunately, the difference is almost constant for other solvents (Figure 44). As a result of this study, cyclohexane will be chosen as a solvent for coating of silane because the best surface deposition was achieved with cyclohexane than others according to the reference [31].

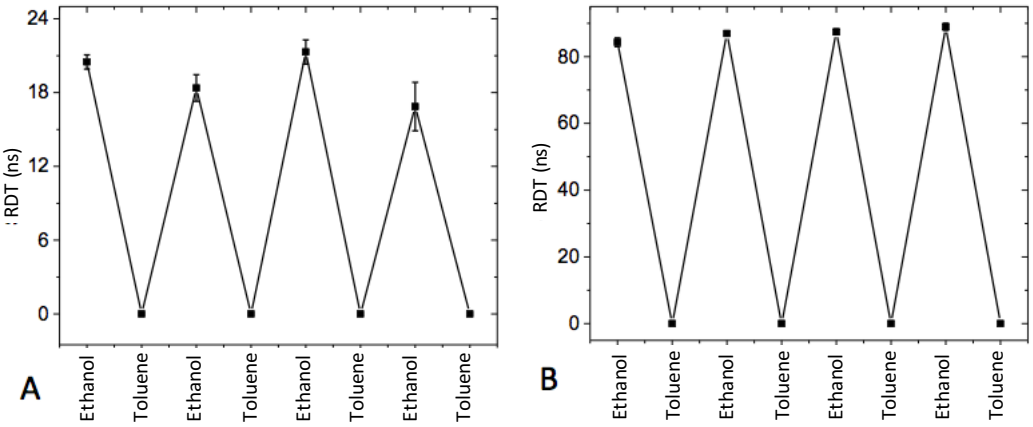


Figure 43. Comparison of RDTs of toluene with ethanol by using different etched fibers (Specifications of etched fiber are: A) 10 μm diameter and 4.0 cm length, B) 8.5 μm diameter and 4.0 cm length )

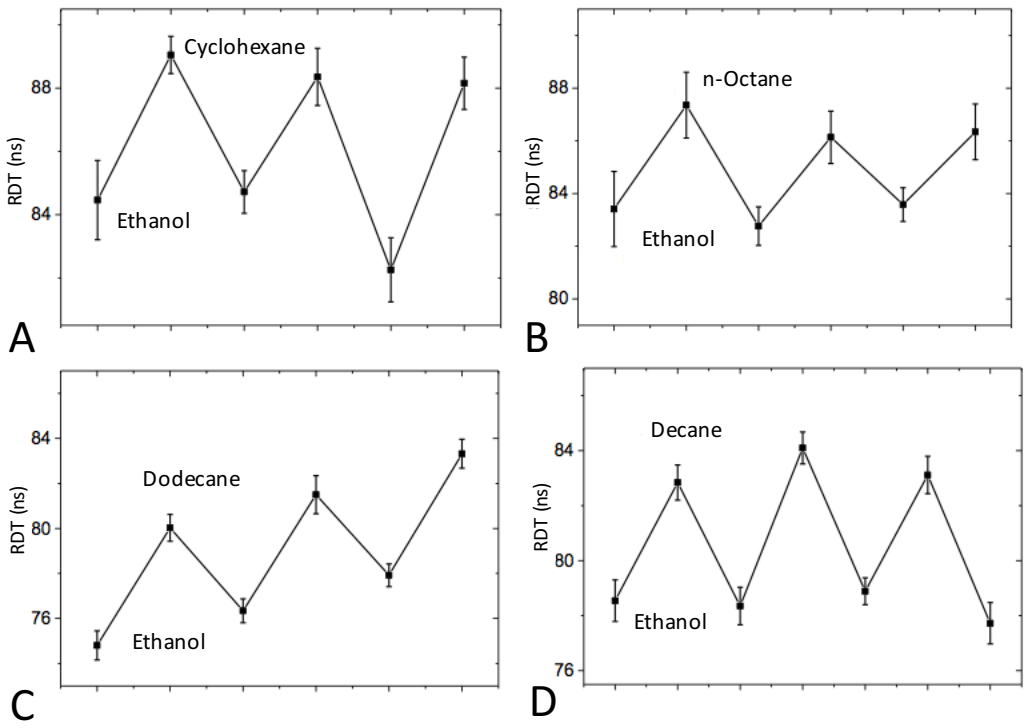


Figure 44. RDTs of selected solvent with respect to ethanol(Whole sample is sensed with 8.5 μm diameter and 4.0 cm length etched fiber after the etched fiber is coated with silane )

3.3.2. Food dyes

In another set of experiments, food dye were used to test the performance of this spectrometer and unique interaction of laser with the samples (by using configuration 2, see detail in Section 2.3.2). There is a change in the RDT of DI water when 5 ml purple dye is mixed in it, as can be seen in Figure 45.A. This change is due to strong absorption of purple food dye in this wavelength. Moreover, for 5 ml purple food dye in 100 ml DI water the effect of absorption in RDT is stronger than that of refractive index change. Next, 1 ml violet in 100 ml DI water was used as sample and this mixture showed higher RDTs than DI water as shown in Figure 45.B. However, violet dye was expected to have a lower RDT than DI water because of its absorption in the operating wavelength. It is believed that refractive index of the solution rises and RDT of the mixture is influenced by

refractive index of the mixture stronger than absorption of the mixture; therefore, higher RDT is measured for violet dye compared to DI water.

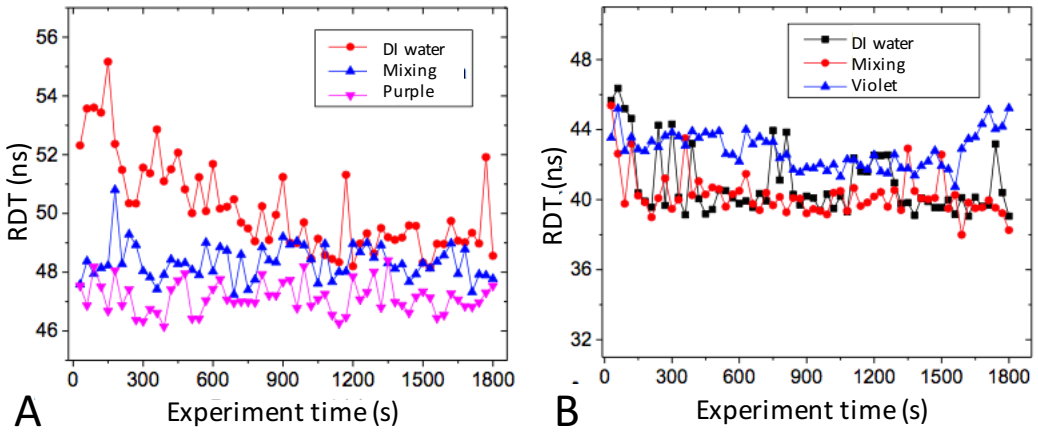


Figure 45. RDTs of purple and violet. (Geometrical parameters of etched fiber in A and B are 35 μm diameter and 9.8 cm length)

### 3.3.3. Polymer coating

After learning the behavior of the spectrometer according to solvents and food dyes, preliminary studies with ultra-thin polymers such as BPEI and PSS for selectivity of the spectrometer were done (The sensing unit has configuration 2, see detail in Section 2.3.2). The experimental part for coating etched fiber with polymers are mentioned in Section 2.3.3. Figure 46 shows that RDT rises after 5 bilayer coatings of etched fiber with BPEI and PSS. However, in the same figure, RDT does not change between 5 and 10 bilayer coating anymore. The thickness of coating determined by using the reference silicon wafers placed in the same solution are presented in Table 9.

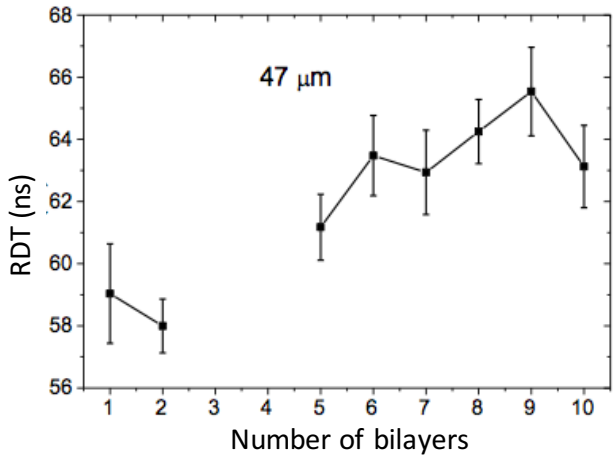


Figure 46. RDTs of layer-by-layer films of BPEI and PSS with etched fiber of 47 μm diameter and 6.1 cm length.

Table 9. Thickness of Si wafers before and after coating

| | **1st Si wafer** | | | **2nd Si wafer** | | |
|---|---|---|---|---|---|---|
| | **Thickness (nm)** | **Fit error (nm)** | **RMS** | **Thickness (nm)** | **Fit error (nm)** | **RMS** |
| Before coating | 1.77 | 0.23 | 0.05 | 3.33 | 0.25 | 0.04 |
| After 3rd bilayer coatings | 26.51 | 0.24 | 0.29 | 27.68 | 0.23 | 0.25 |
| After 10th bilayer coatings | 83.11 | 0.37 | 0.66 | 93.57 | 0.027 | 1.06 |

A similar experiment for coating polymers was also performed with a thinner etched fiber (31.5 μm diameter and 4 cm length). The result shows that RDT of first bilayer coating is lower than reference solution (0.01 M $NaH_2PO_4$, Figure 47.A). Moreover, RDT of second bilayer coating is lower than both first and reference measurements. Almost similar RDTs are observed, however, after 3rd bilayer as can be seen in the same figure. The same procedure is performed in

another experiment with 15 µm diameter and 4 cm length etched fiber. Figure 47.B shows that 4th bilayer coating has different RDT value than that of the fiber in reference solution before and after coating. However, the same RDTs for beginning (before coating, in reference solution) and end (after coating 4 bilayers, in reference solution) mean that RDT after coating does not change with respect to uncoated fiber. However, this study may be used to get the optical properties of the polymers when RDT of polymers are measured during the coating.

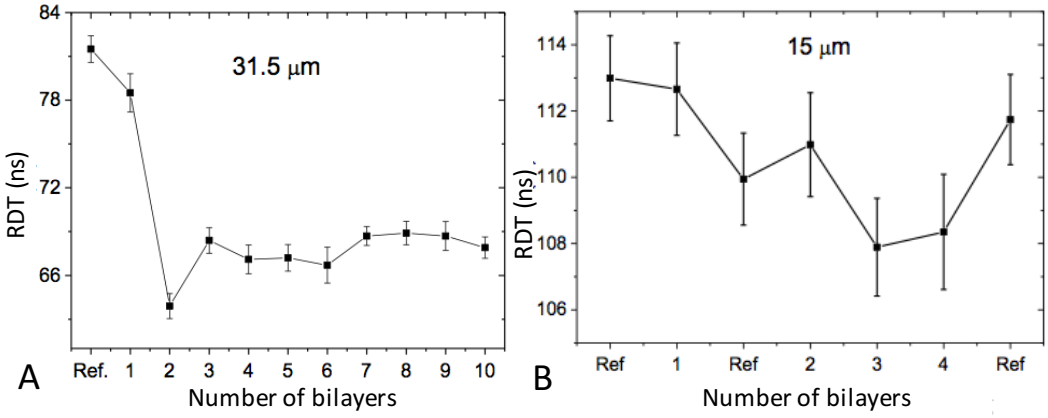


Figure 47. RDTs of layer-by-layer films of BPEI and PSS with etched fiber of 31.5 µm diameter (Panel A) and 15 µm diameter (Panel B)

### 3.3.4. Silane coating

Here, results of etched optical fiber by using configuration 3 (see detail in Section 2.3.2) after silane coating are presented. After polymer coating, this study takes the spectrometer one step further for selectivity and trace chemical detection. The experiment details for this part was presented in Section 2.3.4.

First results show that RDTs were not changed after coating 36.5 µm diameter and 4 cm length etched fibers in toluene (Figure 48). With thinner optical fiber (10 µm diameter and 4 cm length), RDT of toluene is measured as zero because refractive index of toluene is higher than fiber (This result is presented in Section 3.3.1). In this case, there is no internal reflection at the fiber/solvent

surface, so all light escapes out of fiber. Similar experiment is repeated with fiber whose parameters are 8.5 µm diameter and 4 cm length and similar results were observed. Next, silane coating of etched fiber is done in the meantime the RDTs are measured, but it is not seen any difference in RDT signals after and before coating (Both show zero RDTs). In the same experiment, silicon wafer and silica lam are coated in the same beaker where optical fiber is. Afterward, the contact angle of silica lam and silicon wafer are measured and the results demonstrate that surfaces of them behave as dewetting after coating in spite of water drop wets the surface before coating. Moreover, ellipsometer is used to measure the thickness of film on the silicon wafer. The results of silicon wafers show that a few nm thick silane film is deposited. To see effect of silane coating in RDT, solvents having lower refractive index than fiber's are chosen for coating silane. Next, RDT of solvents such as cyclohexane, n-octane, dodecane and decane are inspected with silane coated fiber (4 cm length and 8.5 µm diameter etched fiber). In this study, optical responses of these solvent are compared with ethanol because of volatility of ethanol and its easy-cleaning. The RDTs of these solvent are presented and discussed in Section 3.3.1.

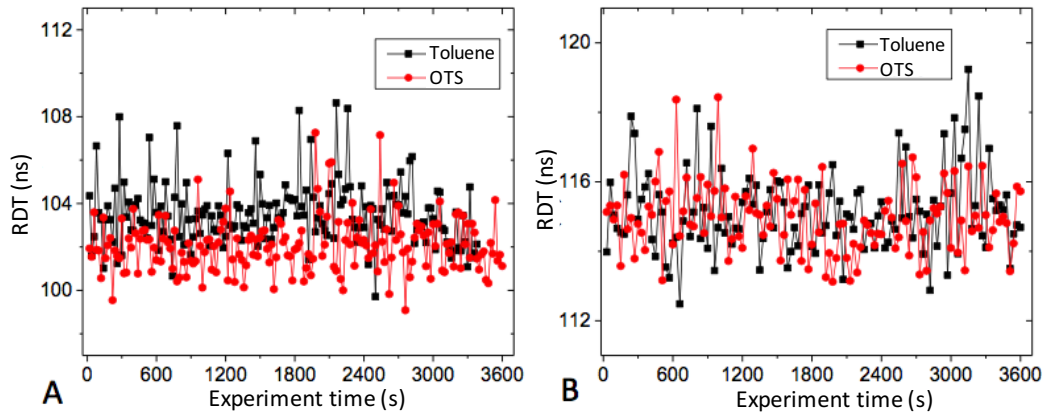


Figure 48. RDTs with different etched fibers before and after silane coating.

As a result, in this section, the unique FLRD-EF spectrometer with 800 nm laser is presented and it is known that there is no similar spectrometer having similar set-up configuration and laser wavelength in literature. With this spectrometer, RDT of acetone, ethanol, DI water, DMSO, DMF, n-butanol, isopropanol, toluene, cyclohexane, n-octane, dodecane and decane are measured and results of these samples are added to literature. Furthermore, less than 1 percentage violet food dye concentration is sensed based upon optical properties of the mixture. Next, polymer is deposited on the etched fiber and one bilayer thick polymer is detected with this spectrometer. Lastly, coating of silane on etched fiber is done and suitable solvent for coating silane is found.

# CHAPTER 4

# CONCLUSIONS

As a result, a low-cost, easy to build, and robust FLRD spectrometer with 1534 nm laser source designed for chemical sensing is presented. The spectrometer sensing region allows real time measurement of a chemical in a mixture environment. Its closed structure enables to increase concentration of analyte simply by increasing the pressure. Stability of the spectrometer was tested with $N_2$ and deviation was found to be only 0.043%. The spectrometer chemical sensitivity is demonstrated with acetylene detection in $N_2$. While the concentration dependence of ring down time deviates slightly from linearity at high concentrations, for low concentrations it is linear. The absorbance plot clearly shows that the 0.1% (v/v) acetylene could be distinguished well from pure $N_2$. Limit of detection was estimated to be 0.1% using the calibration curve obtained. The current setup brings advantages compared to those reported in the literature as shorter fiber length, use of only commercially available components, simpler and shorter sensing region design, possibility to work at high sample pressures that enables enrichment of the analyte in the sample region and lowering the detection limit. Because of its compactness and having low detection limit, this spectrometer may be used in-situ applications to detect trace amount of explosive, toxic, and combustible gases.

Moreover, FLRD spectrometer for liquid samples was set-up with the same laser. Etched optical fiber was formed for liquid samples and configuration of sensing units were studied. Then, optical properties of DMF, DMSO, DI water, ethanol, acetone were investigated after integration of etched optical fiber into the spectrometer. The spectrometer allows fast response (5 seconds, that is, one RDT

measurement) for sensing of ethanol and this result is as good as the ones reported in literature. Besides, there is no study with similar spectrometer for detection of DMSO, DMF and ethanol in the literature.

In the second part of the study, an FLRD spectrometer was constructed with 800 nm laser. After etching optical fiber, chemicals such as acetone, ethanol, DI water, DMSO, DMF, n-butanol, isopropanol, toluene, cyclohexane, n-octane, dodecane, and decane could be sensed. Moreover, 0.0018 refractive index unit difference could be discriminated with this spectrometer by using ethanol and acetone as samples. In addition, less than 1%(v/v) violet as an absorber in water solution could be detected. By using 31.5 μm etched fiber, one bilayer of BPEI and PSS coating could be sensed, that is, less than 8 nm thickness of polymer was detected. Silane films were coated onto etched fiber and suitable solvent for coating was determined. Finally, effect of splicing parameters on insertion loss is investigated and a micro cell was constructed with MOF after the splicing parameters were optimized.

The results are very promising towards its use in many areas. Once they are further developed spectrometers may be used to detect toxic, explosive, and poisonous chemicals in defense industry, for humidity monitoring by measuring amount of water vapor content in air as air-conditioning application, to detect atmospheric gases as space application, to characterize materials by using their optical properties for material development.

## REFERENCES


1. Waechter, H., Litman, J., Cheung, A. H., Barnes, J. A. & Loock, H. P. Chemical sensing using fiber cavity ring-down spectroscopy. *Sensors* **10,** 1716–1742 (2010).
2. Wang, C. Fiber loop ringdown - a time-domain sensing technique for multi-function fiber optic sensor platforms: current status and design perspectives. *Sensors (Basel)*. **9,** 7595–621 (2009).
3. Zhou, W., Wong, W. C., Chan, C. C., Shao, L.-Y. & Dong, X. Highly sensitive fiber loop ringdown strain sensor using photonic crystal fiber interferometer. *Appl. Opt.* **27,** 973–982 (1988).
4. Ittiarah, J. V., Sidhik, S. & Gangopadhyay, T. K. Refractometry using evanescent field based fiber loop ringdown spectroscopy. *Sensors Actuators A Phys.* **223,** 61–66 (2015).
5. Li, R. *et al.* Simultaneous Measurement of Force and Temperature by a Multi-Position Fiber Loop Ringdown Sensor Array. *J. Light. Technol.* **33,** 3607–3612 (2015).
6. Qiu, H. *et al.* Multimode fiber ring-down pressure sensor. *Microw. Opt. Technol. Lett.* **49,** 1698–1700 (2007).
7. Gangopadhyay, T. K. *et al.* Detection of chemicals using a novel fiber-optic sensor element built in fiber loop ring-resonators. *Sensors Actuators, B Chem.* **206,** 327–335 (2015).
8. Zhou, X. *et al.* Melamine detection using phase-shift fiber-loop ring-down spectroscopy. *Opt. Commun.* **333,** 105–108 (2014).
9. Tarsa, P. B., Wist, A. D., Rabinowitz, P. & Lehmann, K. K. Single-cell detection by cavity ring-down spectroscopy. *Appl. Phys. Lett.* **85,** 4523 (2004).
10. Herath, C., Wang, C., Kaya, M. & Chevalier, D. Fiber loop ringdown DNA

and bacteria sensors. *J. Biomed. Opt.* **16,** 50501–50503 (2011).

11. Schnippering, M., Neil, S. R. T., Mackenzie, S. R. & Unwin, P. R. Evanescent wave cavity-based spectroscopic techniques as probes of interfacial processes. *Chem. Soc. Rev. Chem. Soc. Rev* **40,** 207–220 (2011).
12. Wang, C. & Herath, C. Fabrication and characterization of fiber loop ringdown evanescent field sensors. *Meas. Sci. Technol.* **21,** 85205 (2010).
13. Liu, G. *et al.* Mie scattering-enhanced fiber-optic refractometer. *IEEE Photonics Technol. Lett.* **24,** 658–660 (2012).
14. Saleh, B. E. A. & Teich, M. C. *Fundamentals of Photonics*. (1991).
15. Fraz, O. Optical sensing with photonic crystal fibers. **459,** 449–459 (2008).
16. Thapa, R., Knabe, K., Corwin, K. L. & Washburn, B. R. Arc fusion splicing of hollow-core photonic bandgap fibers for gas-filled fiber cells. *Opt. Express* **14,** 9576–9583 (2006).
17. Benabid, F., Couny, F., Knight, J. C., Birks, T. a & Russell, P. S. J. Compact, stable and efficient all-fibre gas cells using hollow-core photonic crystal fibres. *Nature* **434,** 488–491 (2005).
18. Brown, R. S., Kozin, I., Tong, Z., Oleschuk, R. D. & Loock, H. P. Fiber-loop ring-down spectroscopy. *J. Chem. Phys.* **117,** 10444–10447 (2002).
19. Shimizu, H. *et al.* Measurement of carbon dioxide concentration by fiber-loop ring-down spectroscopy for continuous remote measurement. *Jpn. J. Appl. Phys.* **53,** 116601 (2014).
20. Zhang, Y. *et al.* Investigation of erbium-doped fiber laser intra-cavity absorption sensor for gas detection. *Opt. Commun.* **232,** 295–301 (2004).
21. Zhao, Y., Bai, L. & Wang, Q. Gas concentration sensor based on fiber loop ring-down spectroscopy. *Opt. Commun.* **309,** 328–332 (2013).
22. Andrews, N. L. P., Litman, J., Stroh, D., Barnes, J. A. & Loock, H.-P. Near-infrared absorption detection in picolitre liquid volumes using amplified fibre loop ring-down detection. *Opt. Fiber Technol.* **19,** 822–827 (2013).
23. Zhao, Y. *et al.* Novel gas sensor combined active fiber loop ring-down and dual wavelengths differential absorption method. *Opt. Express* **22,** 11244 (2014).

24. Brakel, A. Van *et al.* Cavity ring-down in a photonic bandgap fiber gas cell. 1–2 (2008).
25. Kaya, M., Sahay, P. & Wang, C. Reproducibly reversible fiber loop ringdown water sensor embedded in concrete and grout for water monitoring. *Sensors Actuators B Chem.* **176,** 803–810 (2013).
26. Alali, H. & Wang, C. Fiber loop ringdown humidity sensor. *Appl. Opt.* **55,** 8938–8945 (2016).
27. Wang, C., Kaya, M. & Wang, C. Evanescent field-fiber loop ringdown glucose sensor. *J. Biomed. Opt.* **17,** 37004 (2012).
28. Tarsa, P. B., Rabinowitz, P. & Lehmann, K. K. Evanescent field absorption in a passive optical fiber resonator using continuous-wave cavity ring-down spectroscopy. **383,** 297–303 (2004).
29. Polyanskiy, M. N. Refractive Index Database. Available at: http://refractiveindex.info (last accessed on July 15th 2017)
30. Fadeev, A. Y. & McCarthy, T. J. Self-Assembly Is Not the Only Reaction Possible between Alkyltrichlorosilanes and Surfaces: Monomolecular and Oligomeric Covalently Attached Layers of Dichloro- and Trichloroalkylsilanes on Silicon. *Langmuir* **16,** 7268–7274 (2000).
31. McGovern, M. E., Kallury, K. M. R. & Thompson, M. Role of Solvent on the Silanization of Glass with Octadecyltrichlorosilane. *Langmuir* **10,** 3607–3614 (1994).
32. Borzycki, K. & Schuster, K. TOP 1% Selection of our books indexed in the Book Citation Index in Web of Science™ Core Collection (BKCI) Arc Fusion Splicing of Photonic Crystal Fibres.
33. Jiang, Y., Yang, D., Tang, D. & Zhao, J. Sensitivity enhancement of fiber loop cavity ring-down pressure sensor. *Appl. Opt.* **48,** 6082–6087 (2009).
34. Achtermann, H. J., Bose, T. K., Rögener, H. & St-Arnaud, J. M. Precise determination of the compressibility factor of methane, nitrogen, and their mixtures from refractive index measurements. *Int. J. Thermophys.* **7,** 709–720 (1986).
35. Loock, H.-P. & Wentzell, P. D. Detection limits of chemical sensors:

Applications and misapplications. *Sensors Actuators B Chem.* **173,** 157–163 (2012).

36. Yolalmaz, A., Hanifehpour Sadroud, F., Danışman, M. F. & Esenturk, O. Intracavity gas detection with fiber loop ring down spectroscopy. *Opt. Commun.* **396,** (2017).

# APPENDICES

## APPENDIX A

## MATLAB CODE

```
clear all
clc
tic;
jlo=clock;
format long

qwert=0;

if qwert==0
iter=30;          %number of data you want
itertime=30;

cikti1=1;         % Results are exported when cikti1 is 1
cikti2=2;         % Plots are seen when cikti2 is 1
cikti3=1;         % All results are seen on command window when cikti3 is 1
end

if qwert==1
iter=1;           %Number of data you want
itertime=2;       %Period of data

cikti1=2;         % Results are exported when cikti1 is 1
cikti2=1;         % Plots are seen when cikti2 is 1
cikti3=1;         % All results are seen on command window when cikti3 is 1
end

for uro=1:iter
 % Create a VISA-USB object.
interfaceObj = instrfind('Type', 'visa-usb', 'RsrcName',
'USB0::0x0699::0x0401::C001738::0::INSTR', 'Tag', '');

% Create the VISA-USB object if it does not exist
% otherwise use the object that was found.
```

```
if isempty(interfaceObj)
    interfaceObj = visa('TEK', 'USB0::0x0699::0x0401::C001738::0::INSTR');
else
    fclose(interfaceObj);
    interfaceObj = interfaceObj(1);
end

% Create a device object.
deviceObj = icdevice('MSO4104.mdd', interfaceObj);

interface = get(deviceObj, 'Interface');

fclose(interfaceObj);

% Configure the buffer size to allow for waveform transfer.
set(interfaceObj, 'InputBufferSize', 500000);
set(interfaceObj, 'OutputBufferSize', 500000);

% Connect device object to hardware.
connect(deviceObj);

% Execute device object function(s).
groupObj = get(deviceObj, 'Waveform');
groupObj = groupObj(1);
while 1
zaman(uro)=toc;
if zaman(uro)>uro*itertime              %Itertime is in second
    break;
end
end
[wb(:,uro),wa(:,uro)] = invoke(groupObj, 'readwaveform', 'channel1');

fclose(interfaceObj);
delete(deviceObj);

end

if cikti1==1
%Import file name
filename10='R1535etchedethanol034.xlsx';          %Raw data name
filename20='P1535etchedethanol034.xlsx';          %Result
end

fprintf('Data collection finished and calculation has just been started.')
for uty=1:iter
    a=wa(:,uty);
```

```
b=wb(:,uty);


for i=1:100000
   if a(i)>-5.6e-7
      c(1)=i;
      break
   end
end

for i=100000:-1:1
   if a(i)<1.1e-4
      c(2)=i;
      break
   end
end


for i=c(1):c(2)
 a1(i-c(1)+1)=a(i);
 b1(i-c(1)+1)=b(i);
end
 data_numb=1000;

%    plot(a1,b1)

 for i=(c(2)-data_numb):c(2)
 odsl(i-c(2)+data_numb+1)=b(i);
 end

 m_mean=mean(odsl);
 s_std=std(odsl);

min_limit=m_mean+10*s_std;
max_limit=m_mean+8*s_std;

% Finding max positive peak
 k=0;
 for i=c(1):c(2)
  if b(i)>k
     k=b(i);
  end
 end
 maxpeak=k;

 %Finding first max positive peak
```

```
   erop=0;
     if maxpeak>1.18
     erop=1;
     end
   % erop is 1 when there are saturated peaks

   z=c(1);
  t=1;
  c(3)=c(2);

while 1
   k=m_mean;
      for i=z:c(3)

         if t==1
           if b(i)>maxpeak

         maxi(t)=i;
         max_valueb(t)=b(i);
         max_valueba(t)=a(i);
         break;
           end
         end

         if b(i)>k
         k=b(i);
         maxi(t)=i;
         max_valueb(t)=k;
         max_valueba(t)=a(i);
     end
 end

      if max_valueb(t)<max_limit
         break
      end

   z=maxi(t)+300;
   c(3)=z+100;
   t=t+1;
   if c(3)>=c(2)
            break;
         end
end
datarate=a(2)-a(1);

% plot(max_valueba,max_valueb,'+r',a,b)
```

```
% Number of saturated peak
olu=0;
for i=2:length(max_valueb)
   if max_valueb(1)*0.95<max_valueb(i)
   olu=olu+1;
   end
end

for i=1:length(max_valueba)-1      %Round trip time calculation
tround(i)=max_valueba(i+1)-max_valueba(i);
end

for i=1:length(max_valueba)-1
   tround1=tround;
end

troundtrip=mean(tround1);
troundtrip_std=std(tround1);
datanumber=troundtrip/datarate;    %Number of data between two peaks

%Background correction
for i=1:length(b)
  b1(i)=b(i)-m_mean;
end

%Background correction
for i=1:length(max_valueb)
  max_valueb1(i)=max_valueb(i)-m_mean;
end

% First peaks
rty55(uty)=max_valueb1(1);

for i=1:length(max_valueb1)-olu-1
   max_valueb11(i)=max_valueb1(i+olu+1);
   max_valueba1(i)=max_valueba(i+olu+1);
end

clear max_valueb1
clear max_valueba

max_valueb1=max_valueb11;
max_valueba=max_valueba1;

clear max_valueb11
```

```
clear max_valueba1

if length (max_valueb1)>2
 [fitresult, gof] = fit( max_valueba', max_valueb1', 'exp1');
 too(uty)=-1/fitresult.b;

 ci = confint(fitresult,0.95);
 sap=(-1/ci(2,2)+1/ci(1,2))/2.;
 orew=length(max_valueb1)-2;
 wer=[12.706 4.303 3.182 2.776 2.571 2.447 2.365 2.306 2.262 2.228 2.201 2.179
2.160 2.145 2.131 2.120 2.110 2.101 2.093 2.086 2.080 2.074 2.069 2.064 2.060
2.056 2.052 2.048 2.045 2.042 2.0399 2.0378 2.0357 2.0336 2.0315 2.0294 2.0273
2.0252 2.0231 2.021 2.01995 2.0189 2.01785 2.0168 2.01575 2.0147 2.01365
2.0126 2.01155 2.0105 2.00945 2.0084 2.00735 2.0063 2.00525 2.0042 2.00315
2.0021 2.00105 2];
 std_sapma_too(uty)=sap/wer(orew);
 R2(uty)=gof.rsquare;
end

if length (max_valueb1)<3
too(uty)=(-
max_valueba(2)+max_valueba(1))/log(max_valueb1(2)/max_valueb1(1));
std_sapma_too(uty)=0;
R2(uty)=1;
end
%  hold on;
%  plot(a,b1)
%  plot(fitresult,max_valueba', max_valueb1')
%  hold off;

if cikti1==1
format long
%Importing part
sheet = uty;
AAAA=[max_valueba',max_valueb1'];
xlswrite(filename20,{'time (second)','Intensity (mV)'},sheet,'A1')
xlswrite(filename20,AAAA,sheet,'A3')
BBBB=[too(uty) std_sapma_too(uty) R2(uty)];
xlswrite(filename20,{'Life time (second)','standard error','R2 of fitting'},sheet,'C1')
xlswrite(filename20,BBBB,sheet,'C3')
end

if cikti2==1
figure(uty);
subplot(2,1,1);
plot(a,b,'g',a,b1,'r');
```

```
title('Green is raw data and red is background corrected');
subplot(2,1,2);
plot(a,b1,'g',max_valueba',max_valueb1','+r');
title('Green is background corrected and red is peak points');
 end

clear BBBB
clear AAAA
clear odsl
clear b
clear a
clear b1
clear b11
clear f
clear f1
clear max_value_ba11
clear max_value_b11
clear max_valueba1
clear max_valueb1
clear max_valueba
clear max_value_b
clear max_i
clear max_i1
clear betw_a
clear betw_b
clear maxi
clear max_valueb
clear max_valueba
clear min_i
clear min_value
clear min_value_ba
clear min_valueba
clear mini
clear minvalue
clear t1
clear t11
clear t2
clear t22
clear tround
clear tround1
clear u
end

pro=0;
for i=1:length(too)
   pro=pro+std_sapma_too(i)^2;
```

```
end
proer=sqrt(pro);

 if cikti1==1
    fre=1:length(too);
    sheet = uty+1;
    AAAA1=[fre' zaman' too' std_sapma_too'];
    xlswrite(filename20,{'Times','data taken time','Too (s)','standard error of
fit'},sheet,'A1')
    xlswrite(filename20,AAAA1,sheet,'A3')
    BBBB1=[mean(too) std(too) proer];
    xlswrite(filename20,{'mean','standard deviation','propogation of
error'},sheet,'F1')
    xlswrite(filename20,BBBB1,sheet,'F3')

   sheet = uty+2;
    DDRT=[zaman' rty55'];
    xlswrite(filename20,{'times','Max peak'},sheet,'A1')
    xlswrite(filename20,DDRT,sheet,'A3')
    end
  if cikti3==1
    too'
    std_sapma_too'
 end

clear a
clear b
clear urr

for urr=1:iter
sheet = urr;
a=wa(:,urr);
b=wb(:,urr);
AA=[a b];
 if cikti1==1
xlswrite(filename10,{'time (second)','Intensity (mV)'},sheet,'A1')
xlswrite(filename10,AA,sheet,'A3')
end
 end
 if cikti1==1
     sheet = uty+1;
    CCC=[toc jlo];
    xlswrite(filename20,{'total elapsed time','real time'},sheet,'J1')
    xlswrite(filename20,CCC,sheet,'J3')
 end
```

## APPENDIX B

## THE CODE FOR DECISION OF FIBER LOOP LENGTH

```
clear all
clc
n=1.44;                    % Effective refractive index of fiber
c=3e8;
L=1:2:50000;                    % Length of fiber
tr=n*L/c;
dBTf=0.35*L/1000;
Ti=0.99;                   %Transmission due to isolator
Tc=0.99;                   %Transmission due to coupler
dBTco=1.0;                 %Total loss in dB due to two collimators
Tf=10.^(-dBTf/10);         %Transmission due to fiber optic cable
Tco=10^(-dBTco/10);        %Transmission due to two coupler

Trt=Tf.*Ti*Tc*Tco;         %Total transmission due to total items
too=tr./(-log(Trt));
figure(1);
plot(L,too,'+')
xlabel('Length of fiber loop (m)');
ylabel('Ring down time (s)');
Npeak=5*too./tr;           %It is assumed that the latest peak point is seen
                           when its time equals to 5 times of ratio of RDT to
                           round trip time
figure(2);
plot(L,Npeak,'*')
```

```
xlabel('Length of fiber loop (m)');
ylabel('Number of peak points');
w=[L' Npeak' too'];
```

## APPENDIX C

## THE SENSOR LIMITS FOR ACETYLENE GAS

The limit of detection was calculated as follows: the lowest absorbance difference ($S_y$) was found as 0.000059823 for 0.1 % acetylene concentration at 54.7 and 64.6 psia. At 95 % confidence interval, student-t value (t) is 4.303 for 3 sample measurements and slope of absorbance (r) is 0.00264 (See Figure 36 ). By using these values, limit of detection was found as 0.097506 psia and it corresponds to %0.1 acetylene in nitrogen at 65 psia.

Limit of detection $=t*S_y/r$ [35]

Limit of detection $= 4.303*0.000059823/(0.00264\ psia^{-1})$

$=0.097506$ psia